

Paleoceanography and Paleoclimatology



RESEARCH ARTICLE

10.1029/2021PA004341

Key Points:

- The Cordilleran Ice Sheet (CIS) expansion created high nutrient low chlorophyll conditions
- Biogeochemical changes in the Gulf of Alaska follow 400 and 100 kyr eccentricity cycles
- Increased marine productivity export contributed to the atmospheric CO₂ drawdown and further CIS expansion

Supporting Information:

Supporting Information may be found in the online version of this article.

Correspondence to:

M. L. Sánchez Montes,
m.sanchez-montes@uea.ac.uk

Citation:

Sánchez Montes, M. L., Romero, O. E., Cowan, E. A., Müller, J., Moy, C. M., Lloyd, J. M., & McClymont, E. L. (2022). Plio-pleistocene ocean circulation changes in the Gulf of Alaska and its impacts on the carbon and nitrogen cycles and the Cordilleran Ice Sheet development. *Paleoceanography and Paleoclimatology*, 37, e2021PA004341. <https://doi.org/10.1029/2021PA004341>

Received 28 JUL 2021

Accepted 21 JUN 2022

Author Contributions:

Conceptualization: Maria Luisa Sánchez Montes, Erin L. McClymont

Data curation: Maria Luisa Sánchez Montes

Formal analysis: Maria Luisa Sánchez Montes, Oscar E. Romero

Funding acquisition: Maria Luisa Sánchez Montes, Erin L. McClymont

Investigation: Maria Luisa Sánchez Montes, Erin L. McClymont

Methodology: Maria Luisa Sánchez Montes, Oscar E. Romero, Juliane Müller, Christopher M. Moy, Erin L. McClymont

Project Administration: Erin L. McClymont

© 2022. The Authors.

This is an open access article under the terms of the [Creative Commons Attribution License](https://creativecommons.org/licenses/by/4.0/), which permits use, distribution and reproduction in any medium, provided the original work is properly cited.

Plio-Pleistocene Ocean Circulation Changes in the Gulf of Alaska and Its Impacts on the Carbon and Nitrogen Cycles and the Cordilleran Ice Sheet Development

Maria Luisa Sánchez Montes^{1,2} , Oscar E. Romero^{3,4} , Ellen A. Cowan⁵ ,
 Juliane Müller^{3,4}, Christopher M. Moy⁶ , Jeremy M. Lloyd¹ , and Erin L. McClymont¹ 

¹Department of Geography, Durham University, Durham, UK, ²School of Environmental Sciences, University of East Anglia, Norwich, UK, ³MARUM—Center for Marine Environmental Sciences, University of Bremen, Bremen, Germany, ⁴Alfred Wegener Institute Helmholtz Center for Polar and Marine Research, Bremerhaven, Germany, ⁵Department of Geological and Environmental Sciences, Appalachian State University, Boone, NC, USA, ⁶Department of Geology, University of Otago, Dunedin, New Zealand

Abstract The modern Gulf of Alaska (GOA) is a Cordilleran Ice Sheet (CIS) region, estimated to be important for nutrient cycling and CO₂ exchange. Little is known of the GOA evolution over the Pliocene and Pleistocene as well as its impact on the CIS development, when other evidence for changing North Pacific circulation has emerged. We analyzed Integrated Ocean Drilling Program Expedition 341 Site U1417 sediments, which extend through the Plio-Pleistocene transition (4–1.7 Ma), focusing on productivity-related biomarkers (alkenones, brassicasterol), siliceous microfossils and bulk carbon and nitrogen stable isotopes. Our results show two dominant water column regimes: one characterized by high silica and low organic matter (OM) preservation, containing microorganism remains from a mix of habitats (4–3.7 Ma) and a second characterized by low biogenic silica and increased OM preservation of microorganisms from dominantly open ocean habitats (3.33–3.32 Ma and 2.8–1.66 Ma). An increase of phytoplankton diversity (3.7–3.35 Ma, 3.19–2.82 Ma) characterizes the two transitions of water column conditions, from oxygenated to reductive, that we attribute to a change from ocean mixing to strong stratified conditions with some occasional mixing. The biogeochemical changes in the GOA follow 400 and 100 kyr eccentricity cycles which are also reflected in changes in the CIS. We conclude that the CIS expansion created high nutrient low chlorophyll conditions in the GOA during the Mid Piacenzian Warm Period and the early Pleistocene. In turn, positive feedbacks increased marine productivity export, atmospheric CO₂ drawdown and further CIS expansion.

1. Introduction

During the Pliocene and Pleistocene transition (PPT) and intensification of the Northern Hemisphere Glaciation (iNHG, ~2.6 Ma), changes to marine productivity export patterns have been recorded by means of biogenic silica and alkenone sediment concentrations and linked to changing ocean circulation. In the subarctic Pacific (Haug et al., 2005; Studer et al., 2012), Bering Sea (März et al., 2013), Southern Ocean (Sigman et al., 2004) and parts of the North Atlantic (Lawrence et al., 2009, 2013) marine productivity export is higher before the iNHG. In contrast, other parts of the North Atlantic (Site 607; Lawrence et al., 2013), in the South Atlantic (Cortese et al., 2004; Martínez-García et al., 2010) and the equatorial Pacific (Lawrence et al., 2006, 2013; Liu et al., 2008) the marine productivity export is higher after the iNHG. The different patterns in marine productivity export during the iNHG has been suggested to derive from changes in nutrient distribution (Etourneau et al., 2012) and the equatorial migration of the westerly winds (Lawrence et al., 2013). It has been observed that higher atmospheric CO₂ concentrations occurred when the Southern Ocean and North Pacific were well ventilated (Etourneau et al., 2012) during the warm mid-Pliocene (3.5–3.0 Ma). The development of polar stratification over the PPT, and the resulting limitation in surface ocean macronutrient availability to fuel marine productivity, could have restricted ocean-atmosphere CO₂ exchange in the North Pacific, impacting the climate globally (e.g., Etourneau et al., 2012; Haug et al., 2005). Although these changes have been observed in the northwestern Pacific and Bering Sea (Haug et al., 2005; März et al., 2013), it remains unclear how marine productivity in the northeast Pacific changed over the PPT.

Here, we reconstruct marine productivity changes in the Gulf of Alaska (GOA), northeast Pacific, through the mid- and late-Pliocene and early Pleistocene (4.0–1.7 Ma), analyzing sediments from the Integrated Ocean

Resources: Maria Luisa Sánchez Montes

Supervision: Christopher M. Moy,
Jeremy M. Lloyd, Erin L. McClymont

Visualization: Maria Luisa Sánchez
Montes

Writing – original draft: Maria Luisa
Sánchez Montes

Writing – review & editing: Oscar E.
Romero, Ellen A. Cowan, Juliane Müller,
Jeremy M. Lloyd, Erin L. McClymont

Drilling Program (IODP) Expedition 341 Site U1417 (Figure 1). The proximity of the GOA to the Cordilleran Ice Sheet (CIS, Figure 1), which expanded over this time interval (Gulick et al., 2015; Huber & Bahlburg, 2021; Sánchez-Montes et al., 2020), allows direct examination of how the evolution of a large ice mass affects the supply of macro/micronutrients via fluvial and glacial transport to the ocean to influence marine productivity (Müller et al., 2018). Based on previous research (Haug et al., 2005; Lawrence et al., 2013), one hypothesis is that the marine productivity in the subarctic Pacific was higher before the iNHG due to increased deep nutrient mixing. However, we have previously shown that some biomarkers for marine production at Site U1417 (aquatic *n*-alkane, Sánchez-Montes et al., 2020) suggest an increase in marine productivity in the GOA after the iNHG water column stratification, which might suggest increasing nutrient availability linked to the intensification of the glaciation. It is important to differentiate between these hypotheses, because marine productivity and a change in the North Pacific circulation can have an impact on atmospheric CO₂ concentrations and shifts in climate (e.g., Williamson & Holligan, 1990). Here, we examine aquatic productivity changes over iNHG using a multi-proxy approach by focussing on evidence for marine productivity export through a combination of diatom assemblages (i.e., Katsuki et al., 2003), alkenones (haptophyte algae, Marlowe et al., 1984), brassicasterol (diatoms, Kanazawa et al., 1971; haptophytes, Volkman, 1986) aquatic *n*-alkanes (algae and cyanobacteria, Bourbonniere & Meyers, 1996; Han & Calvin, 1969) and both the accumulation rate and isotopic composition of nitrogen and organic carbon (Addison et al., 2012; Burdige, 2005, 2007; Hedges & Keil, 1995; Walinsky et al., 2009). We combine these approaches with evidence for inputs of terrestrial organic matter (OM) from dust/river/glacial sediment using terrigenous *n*-alkanes (Rieley et al., 1991) and previously published glacier inputs (IRD and %C_{37:4} alkenone, Sánchez-Montes et al., 2020), to assess whether changes to terrestrial nutrient supply also occurred.

2. Research Site

The main GOA oceanographic features include the Alaskan Current (AC) and the Alaskan Coastal Current (ACC) (Figure 1). The AC travels north along the North American west coast and is sourced in warm mid-latitude currents in the North Pacific traveling eastwards around 45°N as the North Pacific Current (NPC). Site U1417 (56°57.58' N, 147°6.58' W; water depth 4,218 m) is currently located under the influence of the AC, characterized by iron-limited, nitrate-rich, low chlorophyll waters in a High Nutrient Low Chlorophyll (HNLC) region (Martin & Fitzwater, 1988; Martin et al., 1991; Hinckley et al., 2009, Figure 1). Productivity in the HNLC region at the center of the Alaska Gyre requires advection of deep, nutrient-rich waters to reach the surface, which reaches a maximum when the Aleutian Low (AL) is centered in the GOA during winter (Figure 1), and when micronutrients (e.g., iron) are supplied from land. Alaskan glacial iron input to the GOA is aided by strong winds associated with the AL in the GOA during autumn (Schroth et al., 2017) but reaches a maximum during August, when Alaskan glacio-fluvial sediments are exposed (Crusius et al., 2011). Asian dust has also been found in the St. Elias Mountains during early April storm events and increased westerly winds (Zdanowicz et al., 2006). Coccolithophorids and diatoms appear as the main phytoplankton groups in the GOA, the former being able to cope with small iron inputs but not able to compete with the latter when iron is available (Martin et al., 1989). The AC later forms the Alaska Stream (AS) when exiting the GOA traveling westwards. The ACC travels northwards along the coast of southwest Alaska toward the Aleutian Arch and to the Bering Sea. A low nutrient high chlorophyll (LNHC) regime dominates under the influence of the ACC closer to coastal Alaska (Whitney et al., 2005). Productivity in the LNHC region requires downwelling relaxation and advection of deep nutrient rich waters for macronutrient availability (e.g., nitrate) into the surface ocean (Figure 1). The ACC is characterized by its low salinity due to the incorporation of glacial and river discharge into the GOA, which is maximum during summer (Figure 1). At present, meltwater is transported along the coastal GOA through the ACC (Kipphut, 1990).

3. Materials and Methods

3.1. Age Model, Sedimentation Rates and Recovered Sediment at Site U1417

This study analyzed Site U1417 sediment depths between 417.3 and 212.2 m CCSF-A dating from 4.0 to 1.66 Ma. The age model and calculated sedimentation rates used in this study are based on the shipboard age model (Jaeger et al., 2014) assuming an even distribution of the recovered material between top and bottom cores when the recovery was incomplete (see Sánchez-Montes et al., 2020; Table S1 in Supporting Information S1). The shipboard age model from 1.66 to 2.2 Ma is well constrained by magnetostratigraphic reversals found in U1417 B or U1417D (C2n(T) Olduvai top, C2n(B) Olduvai base, C2r.1n (T) Reunion top and C2r.1n (B) Reunion base) and

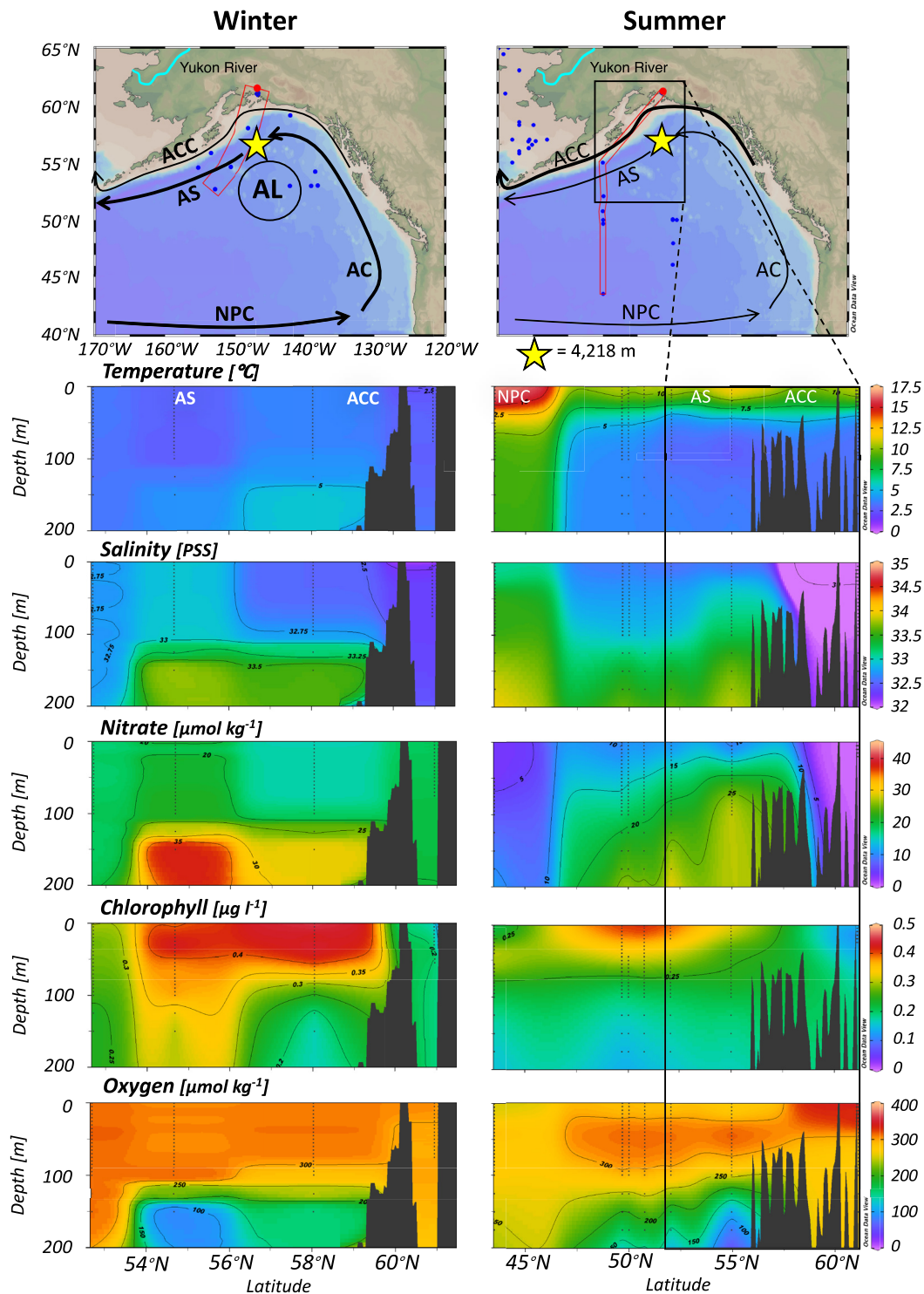


Figure 1. Modern ocean currents and onshore to offshore water properties in the Gulf of Alaska (GOA). Map of the GOA showing data collection sites (blue dots) and selected transect (red rectangle, upper panels) that give rise to the vertical plots; temperature ($^{\circ}\text{C}$) salinity (pss), nitrate ($\mu\text{mol kg}^{-1}$), chlorophyll ($\mu\text{g l}^{-1}$) and oxygen ($\mu\text{mol kg}^{-1}$) during winter (F-M, left) and summer (J-A-S, right). ACC = Alaska Coastal Current, AC = Alaska Current, AS = Alaska Stream, NPC = North Pacific Current, AL = Aleutian Low. The location of site U1417 is indicated with yellow stars and the River Yukon is represented in blue in the upper panels. Data downloaded from World Ocean Database (Boyer et al., 2013), bathymetry data downloaded from GEBCO (GEBCO, 2020) and plotted with Ocean Data View (Schlitzer, 2016). The Cordilleran Ice Sheet (CIS) would occupy the highest Alaskan topography (darker brown colors) of Wrangell-St. Elias and McKenzie Mountains, partially the Yukon and Tanana upland and Olgivine Mountains during the Pliocene-early Pleistocene (2.9–2.6 Ma, Duk-Rodkin et al., 2004).

sediment recovery in this section is close to 100% (Jaeger et al., 2014). This section of the age model remains unchanged in the modified age model used by Sánchez-Montes et al. (2020) and the age errors adopted here from Jaeger et al. (2014) account to ± 0.02 Ma, with a propagated error across neighboring samples of ± 0.028 Ma. For the sediment record older than 2.2 Ma (288.45 m) sediment recovery reduces significantly (70%–12%; Jaeger et al., 2014). The revised age model redistributes this material across the core sections assuming no loss in material (Sánchez-Montes et al., 2020). The age model adjustments resulted in a similar age/depth of the C2r.2r (B) Gauss/Matuyama top (found in U1417 B, D and E), however, C2An.3n (B) Gilbert/Gauss transition found only in U1417D shifted from 408.26 to 410.75 m CCSF-A and from 3.75 to 3.88 Ma (Jaeger et al., 2014; Sánchez-Montes et al., 2020). While the depth error remains the same, the age error over this section of the core has been increased to ± 0.12 Ma to take the Gilbert/Gauss transition age shift into account, with a propagated error across neighboring samples between ± 0.23 to ± 0.69 Ma. There are no big shifts in between the sedimentation rates calculated from the age model of Jaeger et al. (2014) and our stretched age model, which give confidence that our proposed age model only refines the shipboard age model (Sánchez-Montes et al., 2020). Beyond 3.88 Ma U1417's age model is poorly constrained due to poor core recovery (see Jaeger et al., 2014; Sánchez-Montes et al., 2020) and, therefore, it determines the lower age range of this study to 4 Ma.

Uncertainty of the age model and sedimentation rates presented here follow the polarity chronozone interpretations of the shipboard age model (Gulick et al., 2015; Jaeger et al., 2014) and accounts for shifts in the Gilbert-Gauss magnetic reversal in the adjusted age-depth model (Sánchez-Montes et al., 2020, Table S1 in Supporting Information S1). The sedimentation rates are calculated across our analyzed samples, almost exclusively in Hole U1417D. Sedimentation rates increase during the mid and late Pliocene (from 40 to 85 m/Myr across 3.5–2.8 Ma), and during the iNHG increase in glaciogenic inputs (from 85 to 156 m/Myr at 2.4 Ma). Our manually calculated sedimentation rates on the CCSF-A scale across neighboring samples follow the depth-age model uncertainties of Jaeger et al. (2014) but differ slightly from the shipboard age model, where average sedimentation rates are calculated over 0.5 Myrs following the CCSF-B scale, and uncertainties ($+1\sigma$) are calculated using a Monte-Carlo sedimentation model over the whole Site U1417 (Jaeger et al., 2014). After distributing the sediment evenly across the core (Sánchez-Montes et al., 2020), our calculated sedimentation rate uncertainties become smaller when compared to the statistical approach of the shipboard age model (Jaeger et al., 2014). The sediments recovered include diatom ooze interbedded with debris flow deposits containing mud clasts and plant fragments (lithostratigraphic unit VA, 4–3.2 Ma), marine mud (unit IV and II, 3.2–2.8 Ma and 2.4–1.66 Ma) and ice-rafted diamict interbedded with mud (unit III, 2.8–2.4 Ma; Jaeger et al., 2014). Samples for organic matter analyses were selected avoiding sand, silt, ash or gravel (e.g., Ausín et al., 2019, 2021).

3.2. Carbon and Nitrogen Bulk and Isotope Analyses

Approximately 70 mg of freeze-dried and homogenized sediment was weighed into silver capsules and acidified in-situ with 5%–6% sulfurous acid (H_2SO_3) to remove carbonate phases (Verardo et al., 1990). Additional aliquots of acid were repeated until no reaction was observed using a binocular microscope, which ensured removal of inorganic carbon. No method was implemented for inorganic nitrogen removal. Samples were oven-dried between acidifications at 40°C. 6 mg of Tungsten VI oxide (WO_3) was added to each sample to facilitate combustion. Samples were then measured using a Varian elemental analyzer coupled to a Europa Scientific continuous-flow isotope-ratio mass spectrometer. The average standard deviation of replicate samples is 0.58 ‰ for $\delta^{15}\text{N}$, 0.006‰ for total nitrogen (TN), 0.26 ‰ for $\delta^{13}\text{C}$ and 0.031‰ for total organic carbon (TOC) ($n = 8$ pairs). The TOC and TN were normalized to the accumulation rates of the sediment analyzed (Equations 1–3), where “material” refers to TOC or TN:

$$\text{Material (mg g}^{-1}\text{)} = \frac{\text{Mass material (mg)}}{\text{Weight sample (g)}} \quad (1)$$

$$\text{Bulk MAR (g cm}^{-2}\text{kyr}^{-1}\text{)} = \frac{\text{Dry bulk density (g cm}^{-3}\text{)}}{\text{Sedimentation rates (cm kyr}^{-1}\text{)}} \quad (2)$$

$$\text{Material MAR} = \text{Bulk MAR} \times \text{Material} \quad (3)$$

3.3. Siliceous Microfossil Assemblages and Biogenic Silica

Microplaeontological counting standard methods and techniques (Schrader & Gersonde, 1978) were followed to prepare sediments after freeze-drying. Siliceous microfossil species identification and counts were performed on pre-acid cleaned permanent slides (*Mountex*® mounting medium). Several traverses across each slide were examined on a *Zeiss*®Axioscop with interference illumination at x1000 magnifications (MARUM, University of Bremen). Depending on valve abundances, between ca. 400 and ca. 700 valves per slide were counted. Duplicate slide counting quantified the concentration estimate analytical error $\leq 10.0\%$. Counting outputs were converted in sedimentary abundance of individual diatom taxa, total diatom (in valves per g^{-2}) and total silicoflagellate (in skeletons per g^{-2} , Equation 4) which were then converted to mass accumulation rates (MAR, Equation 3). The relative abundance (%) of each species was calculated as the fraction of the diatom species versus the TC in a particular sample (Equation 4).

$$TC = [N] \left[\frac{A}{a} \right] \left[\frac{1}{W} \right] \left[\frac{V}{v} \right] \quad (4)$$

where, TC is the total concentration, [N] is the number of valves in [a], an known area, [A] is the total area of a petri dish, [W] the sample weight in grams, and [V/v] the sample volume of the permanent slide (Sancetta & Calvert, 1988).

Diatom taxa were grouped in 6 palaeo-habitats: benthic, coastal high productivity, coastal moderate productivity, pelagic high productivity, pelagic warm water and freshwater (Table S2 in Supporting Information S1). The coastal high and moderate productivity palaeo-habitats describe coastal diatoms that occur at intervals of high and moderate productivity due to high and moderate nutrient availability in surface coastal waters, respectively. The pelagic high productivity palaeo-habitat is composed by pelagic diatoms that occur at intervals of high productivity and high nutrient availability in surface pelagic waters. The pelagic warm waters is a palaeo-habitat that contains subtropical pelagic diatoms species that thrive in warm waters (Ren et al., 2014), representing the possible northward transport of warm to temperate waters into the GOA. The Shannon Weaver Index (SWI) was calculated to quantify diatom diversity (Shannon & Weaver, 1949).

Diatom preservation is reconstructed to assess whether a water column silica is rich or poor, with longer or lower exposure of silica to degradation due to slower or more rapid sediment burial. Following observations with light microscopy, three main states of valve preservation were defined as: (a) good or no significant enlargement of the areole or dissolution of the valve margin; (b) moderate where valves show areole enlargement, dissolution of the valve margin and valve fragmentation; and (c) poor or strong dissolution of the valve margin and areole enlargement (Crosta et al., 2012; Romero et al., 2005, 2009, 2012, 2015). In addition, two intermediate states of dissolution characterize valves whose state of preservation does not fully fit the three above-mentioned categories: good/moderate (good preservation predominates over moderate preservation) and moderate/good (moderate preservation predominates over good preservation).

Biogenic silica was determined with a sequential leaching technique with 1M NaOH at 85°C (Müller & Schneider, 1993) and normalized to the weight of the sample (wt%) and accumulation rates of the sediment (Equation 3). The precision of the overall method based on replicate analyses varies between ± 0.2 and $\pm 0.4\%$, depending on the material analyzed.

3.4. Biomarker Analyses

The lipid biomarker extraction followed the microwave assisted extraction method of Kornilova and Rosell-Melé (2003), and detailed in Sánchez-Montes et al. (2020). To obtain *n*-alkanes, aromatics, ketone, and polar fractions, total lipid extracts were separated using silica column chromatography through sequential elution with hexane (3 mL), hexane: dichloromethane (9:1; 1.5 mL), dichloromethane (5.5 mL), and ethylacetate: hexane (20:80; four columns) (Sánchez-Montes et al., 2020). Each fraction was analyzed by Gas Chromatography Mass Spectrometry for compound identification, and Flame Ionization Detector (GC-FID) where biomarkers were separated using a 60m \times 0.25 mm i.d., Restek RXi-5ms column (0.25 m 5% diphenyl-95% dimethyl polysiloxane coating). Lipid quantification was achieved with reference to the following internal standards: 5 α -cholestane for *n*-alkanes, 2-nonadecanone for ketones, and 5 α -androstan-3 β -ol for polars (Equation 5), normalized to the original extracted dry weight of sediment and then calculated as mass accumulation rates (MAR), to take into

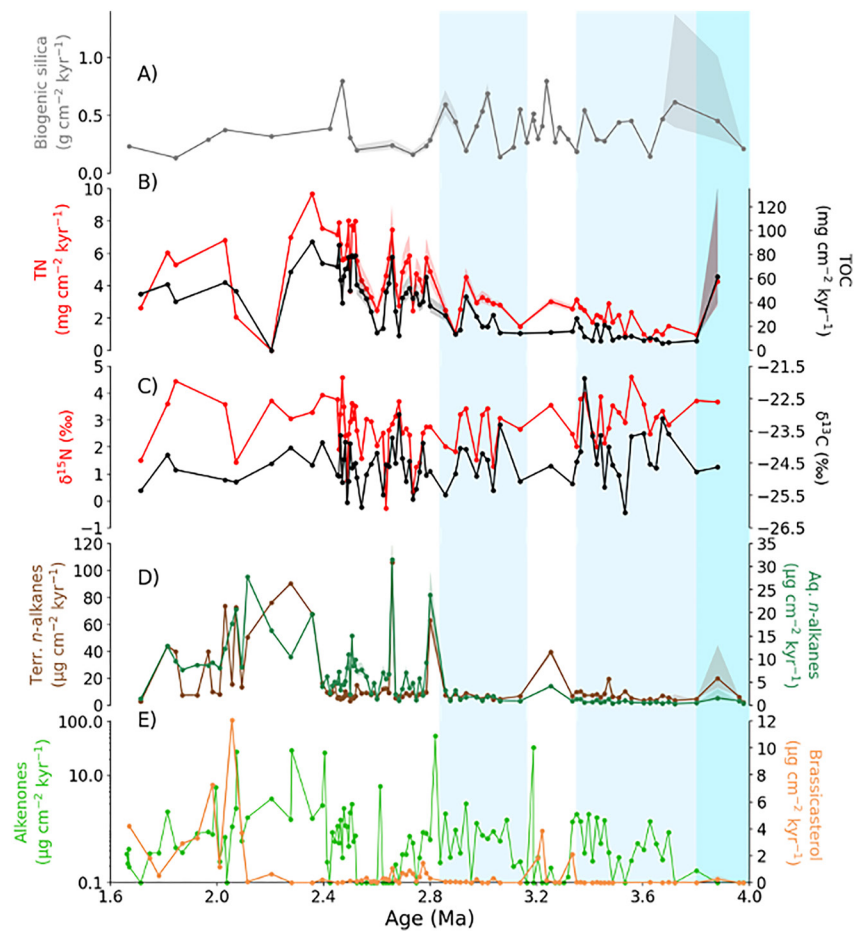


Figure 2. Terrestrial and marine productivity bulk and biomarker results at Site U1417. (a) Biogenic silica mass accumulation rates (MAR) ($\text{g cm}^{-2} \text{kyr}^{-1}$), (b) total nitrogen (red) and total organic carbon MAR (black) ($\text{mg cm}^{-2} \text{kyr}^{-1}$), (c) $\delta^{15}\text{N}$ (red) and $\delta^{13}\text{C}$ (black) (‰), (d) terrestrial (brown) and aquatic (turquoise) *n*-alkanes MAR ($\mu\text{g cm}^{-2} \text{kyr}^{-1}$) and (e) alkenone (green) and brassicasterol MAR (orange) ($\mu\text{g cm}^{-2} \text{kyr}^{-1}$). Shadings indicate uncertainties in MAR associated with the age and depth uncertainties of the tie-points in Jaeger et al. (2014) and age-depth adjustments in Sánchez-Montes et al. (2020) (see Table S1 in Supporting Information S1).

account the influence of changing sedimentation rate and sediment density on original biomarker concentrations (Equation 3).

$$\text{Mass biomarker } (\mu\text{g}) = \left(\frac{\text{Mass standard } (\mu\text{g})}{[\text{Area standard}]} \right) [\text{area biomarker}] \quad (5)$$

4. Results

During the Pliocene-early Pleistocene, biogenic silica export to Site U1417 exceeds TOC by 15 times (Figures 2a and 2b). TOC is overall 10 times more abundant than TN (Figure 2b). As part of the TOC, the sum of long-chain (C_{27} , C_{28} , C_{31}), or terrigenous, *n*-alkanes is overall 3 times higher than that of short chain (C_{15} , C_{17} , C_{21}), or aquatic, *n*-alkanes (Figure 2d). Aquatic *n*-alkane MAR are 2 times higher than alkenone MAR (from haptophyte algae), which, in turn, are 3 times more abundant than brassicasterol (from diatoms and haptophyte) (Figure 2e). The main changes across the PPT (3.2–2.4 Ma) are the overall decrease in biogenic silica MAR, increase in TOC MAR, TN MAR, terrestrial and aquatic *n*-alkane MARs and the decrease and later (2.6 Ma) increase in $\delta^{13}\text{C}$ and $\delta^{15}\text{N}$ (Figure 2). Maxima in *n*-alkanes, alkenones and brassicasterol are observed during the early Pleistocene (2.4–1.7 Ma, Figures 2d and 2e).

Diatoms and silicoflagellate MAR are highest during the early part of the record (4.0–3.8 Ma, Figure 3a), with coastal high productivity diatoms as the most abundant group at Site U1417 followed by benthic, coastal moderate productivity, pelagic warm and freshwater diatoms (Figure 3, Table S2 in Supporting Information S1). Across 3.7 to 2.8 Ma, diatoms and silicoflagellate MAR decrease progressively. Silicoflagellates disappear by 3.35 Ma, whereas diatoms almost disappear by 2.8 Ma (Figure 3a). The diatom assemblages recorded at Site U1417 switch from coastal high productivity to dominantly pelagic high productivity groups across 3.7 to 2.8 Ma (Figure 3, Table S2 in Supporting Information S1), particularly between 3.3 and 3.2 Ma. *Coscinodiscus marginatus*, the main species contributing to the pelagic high productivity assemblage at Site U1417, is a minor component of the diatom communities in the North Pacific across the Cenozoic, but it has been found abundant in the subarctic Pacific and Bering Sea during the Late Pliocene (Shimada et al., 2009).

The preservation of diatoms follows the same stepwise decline as the total diatom abundances, where preservation is high during 4–3.7 Ma, decreases gradually across 3.7–3.2 Ma and increases slightly between 3.19 and 2.8 Ma before diatoms almost completely disappear from the record between 2.8 and 1.7 Ma (Figure 3b). Biogenic silica MAR decreases in response to the decline in diatom MAR at 2.8 Ma (from an average of 0.39 ± 0.05 to $7-0.31 \pm 0.016$ g cm⁻² kyr⁻¹; Figure 3a). The decrease in siliceous microfossils occurs during an increase of organic matter concentrations (TOC and TN) across the PPT (Figure 4). The early Pleistocene increase in organic matter content (Figure 4d) is also evident in the increasing biomarker concentrations (Figures 4a–4c). Signs of different production or selective organic matter degradation are suggested by different patterns in the biomarkers that is, peaks in alkenone often coincide with the absence of sterols (Figures 4a and 4b).

5. Discussion

Across 4.0–1.7 Ma, the marine productivity export to Site U1417 is characterized by changes in the relative contribution of siliceous microfossils and organic matter (Figure 4). These changes culminate with an increase in organic matter export and almost complete disappearance of siliceous remains across the PPT and early Pleistocene (Figure 4). A range of factors could explain the siliceous/organic matter export changes, including (a) changes in nutrient supply and phytoplankton production, (b) water column stratification and carbon/silica preservation, and/or (c) the impact of sedimentation rate on phytoplankton burial efficiency and preservation. Here we examine chronologically the forcings and responses behind the siliceous and organic matter productivity export changes. According to these changes, the record can be divided into three intervals: the early Pliocene (4.0–3.8 Ma), the late Pliocene (3.7–2.82 Ma), and the PPT and early Pleistocene (2.8–1.66 Ma).

5.1. The Early Pliocene (4.0–3.8 Ma): High Biogenic Silica Export of Coastal High Productivity Habitats

The maximum MAR of diatoms (up to 100×10^6 valves cm⁻² kyr⁻¹, Figure 3a) and silicoflagellates (up to 0.3×10^6 valves cm⁻² kyr⁻¹, Figure 3a) suggests increased marine productivity at Site U1417 during the early Pliocene. The high SWI indicates a highly diverse diatom community (Figure 3b) at Site U1417, where diatoms originate from a range of habitats: coastal high productivity, benthic, pelagic high productivity, coastal moderate, pelagic warm and freshwater (from most to least abundant, Figure 3, Table S2 in Supporting Information S1). The biogenic silica concentrations are also high, which accounts for the productivity, preservation and valve sizes of a number of siliceous microorganisms such as diatoms, silicoflagellates and radiolarians, the last two being less abundant at Site U1417 than diatoms.

The most prolific diatoms are *Chaetoceros* resting spores (up to 68×10^6 valves cm⁻² kyr⁻¹, Figure 3c, Table S2 in Supporting Information S1), which are abundant in highly productive coastal waters in the GOA (e.g., Ren et al., 2014). *Chaetoceros* dominate the diatom community of the GOA when iron is added to the North Pacific (Tsuda et al., 2003) and they develop resting spores after nutrient consumption (Margalef, 1978). Therefore, the prolific coastal diatom productivity suggests iron supply from the nearby continent and shelves to the neritic zone of the GOA (e.g., Lam & Bishop, 2008; Ren et al., 2014). The marine productivity species at Site U1417 suggest a productivity gradient during this time, less steep towards the coast compared to present (Figure 1), where the maximum productivity export of diatoms occurs.

The low contribution of pelagic diatoms and marine biomarkers (brassicasterol, alkenones and aquatic *n*-alkane MAR) suggests a limited open-ocean productivity in the GOA (Figures 4a–4c). This causes a contrast between a highly productive coastal zone which supported diatom productivity in coastal habitats to the detriment of

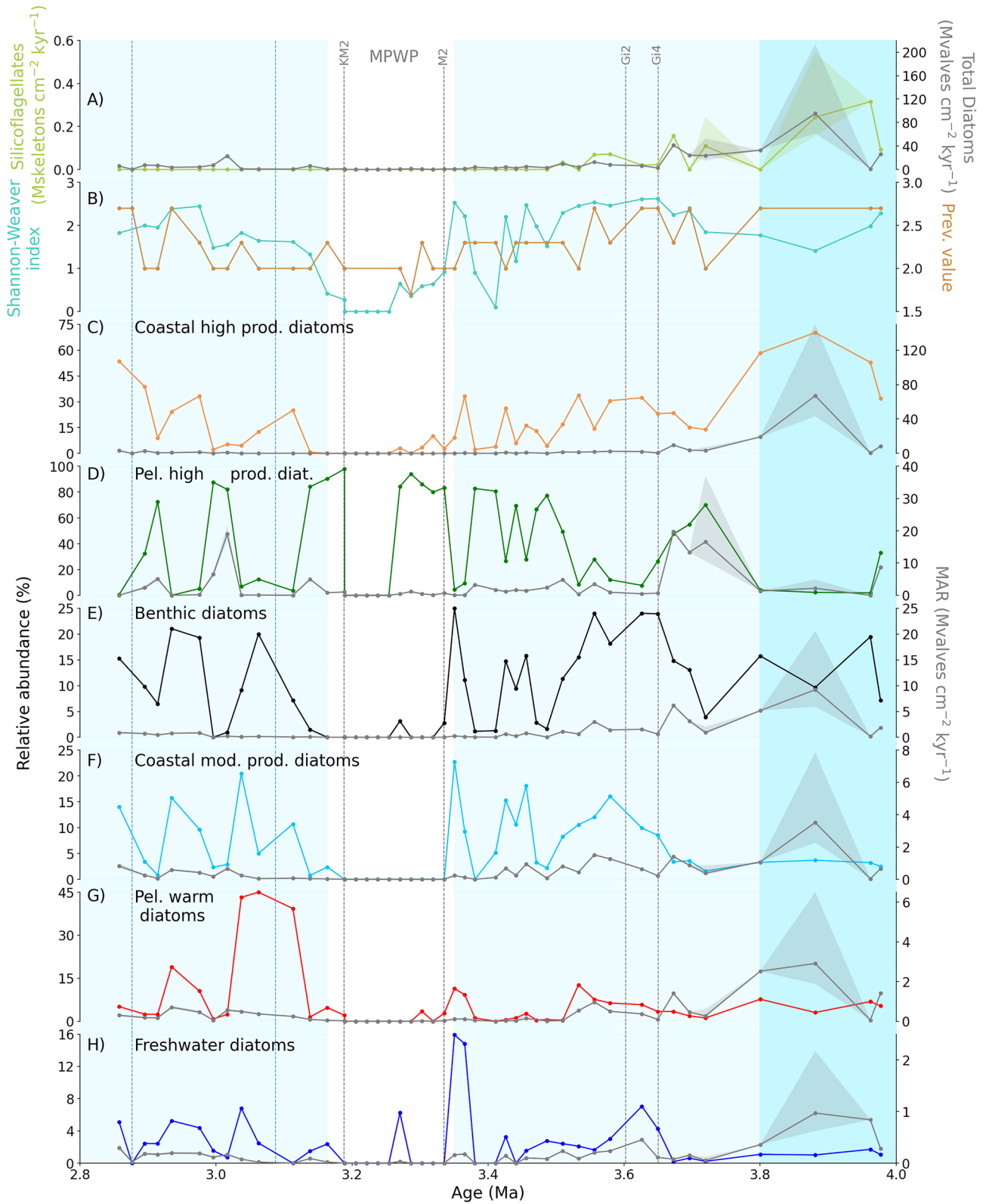


Figure 3.

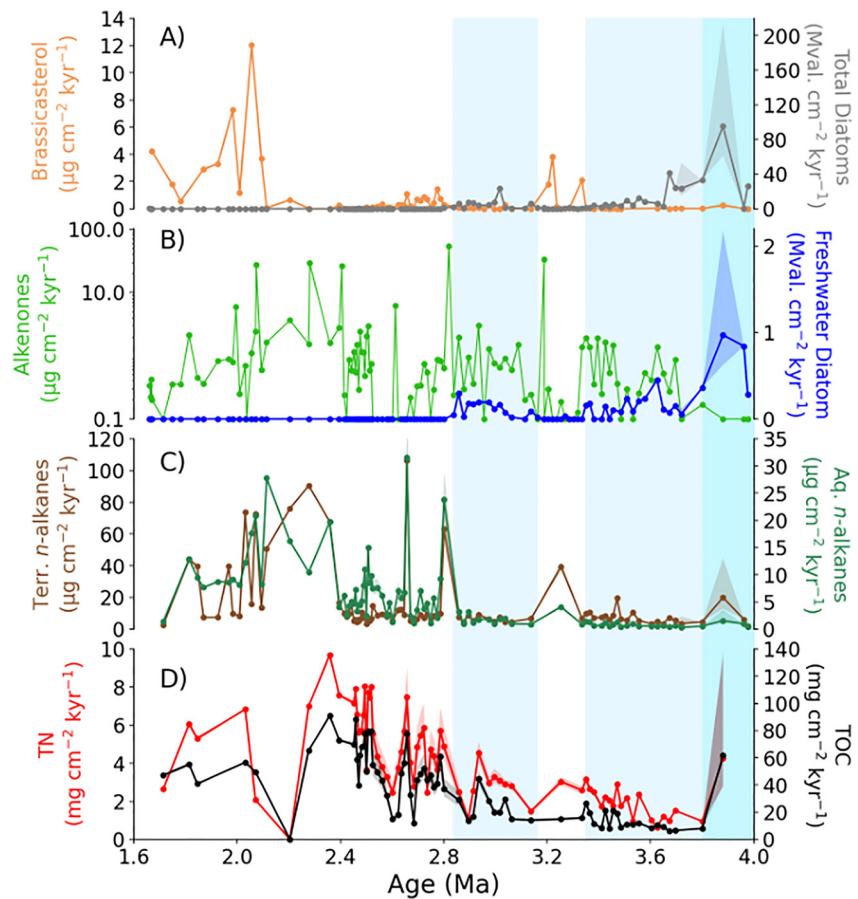


Figure 4. Plio-Pleistocene productivity export and water column ventilation. (a) total diatom (million valves $\text{cm}^{-2} \text{kyr}^{-1}$; gray) and brassicasterol ($\mu\text{g cm}^{-2} \text{kyr}^{-1}$; orange) mass accumulation rates (MAR); (b) freshwater diatom (blue, million valves $\text{cm}^{-2} \text{kyr}^{-1}$; blue) and alkenone ($\mu\text{g cm}^{-2} \text{kyr}^{-1}$; light green; in log scale) MAR; (c) terrigenous (brown) and aquatic (turquoise) *n*-alkane MAR ($\mu\text{g cm}^{-2} \text{kyr}^{-1}$) and (d) total nitrogen (TN; red) and total organic carbon (TOC; black) MAR ($\text{mg cm}^{-2} \text{kyr}^{-1}$) at Site U1417 against age (Ma). Blue vertical shadings indicate higher (deeper blue) and high (light blue) biogenic silica preservation, the rest non-shaded intervals indicate increases in organic matter (OM) preservation (e.g., the Mid Piacenzian Warm Period (MPWP) (3.33–3.19 Ma)). Shadings indicate uncertainties in MAR associated with the age and depth uncertainties of the tie-points in Jaeger et al. (2014) and age-depth adjustments in Sánchez-Montes et al. (2020) (see Table S1 in Supporting Information S1).

pelagic diatom, coccolithophores and other marine phytoplankton productivity (Herbert, 2001). The regime of abundant micro-nutrients and low macro-nutrients known as LNHC characterizes the modern coastal Alaska (Weingartner, 2007). The source of micro-nutrients during the Pliocene could be from two terrestrial sources: glacial flour and/or aeolian dust (Müller et al., 2018; Romero et al., 2022). Iron-rich glacial flour is abundant in modern coastal Alaska estuaries for example, the Copper River (Crusius et al., 2011) and the continental margin (Lam & Bishop, 2008). Wind transport is an important mechanism today for transporting dust from Alaska hundreds of kilometres beyond the shelf break to the GOA (Crusius et al., 2011, 2017). However, high pollen

Figure 3. Detailed Pliocene (4.0–2.8 Ma) marine productivity export at Site U1417. (a) Silicoflagellate (million skeletons $\text{cm}^{-2} \text{kyr}^{-1}$, green) and total diatom (million valves $\text{cm}^{-2} \text{kyr}^{-1}$, gray) mass accumulation rates (MAR); (b) the Shannon-Weaver index of diversity of species (turquoise) and the preservation value (brown); (c) coastal high productivity diatom species relative abundance (%) (orange) and MAR (million valves $\text{cm}^{-2} \text{kyr}^{-1}$, gray); (d) pelagic high productivity diatom species relative abundance (%) (green) and MAR (million valves $\text{cm}^{-2} \text{kyr}^{-1}$, gray); (e) benthic diatom species relative abundance (%) (in black) and MAR (million valves $\text{cm}^{-2} \text{kyr}^{-1}$, gray); (f) coastal moderate productivity diatom species relative abundance (%) (in blue) and MAR (million valves $\text{cm}^{-2} \text{kyr}^{-1}$, gray); (g) pelagic warm diatom species relative abundance (%) (in red) and MAR (million valves $\text{cm}^{-2} \text{kyr}^{-1}$, gray) and (h) freshwater diatoms relative abundance (%; blue) and MAR (million valves $\text{cm}^{-2} \text{kyr}^{-1}$, gray). Vertical lines correspond to glacial stages (gray) and key events on the Cordilleran Ice Sheet (CIS) runoff history (blue, see text). Blue vertical shadings indicate higher (deeper blue) and high (light blue) biogenic silica preservation, the non-shaded interval indicates poor silica preservation. Shadings indicate uncertainties in MAR associated with the age and depth uncertainties of the tie-points in Jaeger et al. (2014) and age-depth adjustments in Sánchez-Montes et al. (2020) (see Table S1 in Supporting Information S1).

abundance at Site U1417 during the early Pliocene suggests higher riverine terrestrial input from coastal Alaska to the GOA (Pisias et al., 2001; Sanchez-Montes et al., 2020). The presence of freshwater diatoms contributing around 1% to the total diatom concentration in the GOA is most likely attributed to Alaskan aeolian dust transport (Figure 4b) (e.g., Crusius et al., 2011; Crusius et al., 2017). Coastal diatoms have been previously interpreted as downslope transport inputs to Site U1417 from the coastal area (Jaeger et al., 2014). Another explanation is the ocean fertilisation by dust nutrient delivery and increase in coastal diatom productivity.

The 30% contribution of benthic diatoms to the total diatom MAR at Site U1417, despite its location at 4,218 m water depth (Jaeger et al., 2014), points to the transport of shallow water habitat assemblages toward the Surveyor Fan (McGee et al., 2008). The early Pliocene lithology at Site U1417 contains gravity flow deposits, while the tectonic history in the GOA and coastal Alaska during the Pliocene (Enkelmann et al., 2015) may result in slope instability and distal transport of shallow species to Site U1417, which lies ~700 km from the coastline (comparable to distances observed in turbidity current transports offshore West Africa, Talling et al., 2007). Relatively high terrestrial *n*-alkane MAR (Figure 4c) suggest enhanced flux of terrestrial OM input and rapid burial during gravity flows, which may also account for the peaks in TOC (e.g., Hage et al., 2020). Plant fragments were also observed at Site U1417, and attributed to both mature (Rea, Basov, Krissek, & the Leg 145 Scientific Party, 1995; Rea, Basov, Scholl, & Allan, 1995; Gulick et al., 2015) and fresh (Jaeger et al., 2014) origins (Sánchez-Montes et al., 2020). High TN (Figure 4d) and $\delta^{15}\text{N}$ values of 3.7‰ (Figure 2c) suggest around 50% terrestrial origin of nitrogen at Site U1417 (Walinsky et al., 2009). In addition to the tectonic framework of the GOA, the presence of freshwater diatoms at Site U1417 (Figure 4b) could support the importance of river transport and glacial development to trigger slope instability and gravity flows (e.g., Hage et al., 2019; Pope et al., 2018).

The early Pliocene contains the highest concentration of benthic and freshwater diatoms (average 15%) known to synthesize brassicasterol (e.g., Piepho et al., 2012; Rampen et al., 2009) found at U1417 (Table S2 in Supporting Information S1), yet brassicasterol concentrations are low during the early Pliocene. Low brassicasterol concentrations could reflect organic matter degradation or less favorable (nutrient) conditions for brassicasterol producers (Goat & Withers, 1982; Kanazawa et al., 1971; Lei et al., 2012; Volkman, 1986, 2006).

The high diatom productivity (high diatom MAR) may have been supported by an abundant ocean carbon pool with widely available ^{12}C , as shown by low bulk $\delta^{13}\text{C}_{\text{org}}$ at this time (-24.7‰ , Figure 2c). A large carbon pool could suggest a very well mixed and oxygenated ocean. An oxygenated water column would also favor silica preservation rather than organic matter preservation, as observed in Site U1417 (Figures 4a and 4b, Figures 5b and 5c). The oxygenated water column, perhaps aided by oxygen transport via turbidity currents, downwelling movement of water masses and ocean mixing, could explain the low concentration of marine biomarkers in the GOA during the early Pliocene (Figure 6). The low sedimentation rates during the early Pliocene might also have favored organic matter degradation at the sediment-water interface due to longer exposure to oxidising conditions outside of the gravity flow events (Figure 4a).

5.2. The Late Pliocene (3.7–2.82 Ma): Decrease in Terrestrial and Coastal Biogenic Silica and Increase in Marine Productivity

The decrease in diatom and silicoflagellate MAR (Figure 3a) during the late Pliocene seems to be caused by a decrease in flux and silica preservation (e.g., Thunell et al., 1994; preservation value, Figure 3b) and is accompanied by an increase in the number of pelagic diatom species (Figure 3d). The main contributor to the total diatom MAR thus shifts from coastal high productivity species during the early Pliocene (average of 54%) to pelagic high productivity species during most of the late Pliocene (average of 56%; Figures 3c and 3d). These ecological changes are accompanied by a higher diatom diversity during the late Pliocene than during the early Pliocene (Figure 3b), which could partially explain a small increase in biogenic silica preservation from the previous period (Figure 2a).

The disappearance of silicoflagellates from the record at 3.35 Ma (Figure 3a) occurs with an increase in organic matter inputs to Site U1417. The progressive increase in productivity indicators from coccolithophores (e.g., alkenones; Figure 4b) and other phytoplankton (aquatic *n*-alkanes, Figure 4c) alongside increasing TOC and TN (Figure 4d) suggests better organic matter preservation and/or increasing export production from marine sources. Terrigenous *n*-alkanes decrease during most of the late Pliocene (Figure 4c) suggesting a reduction in land vegetation and/or a reduced riverine/aerial terrestrial plant transport to Site U1417, also suggested by an

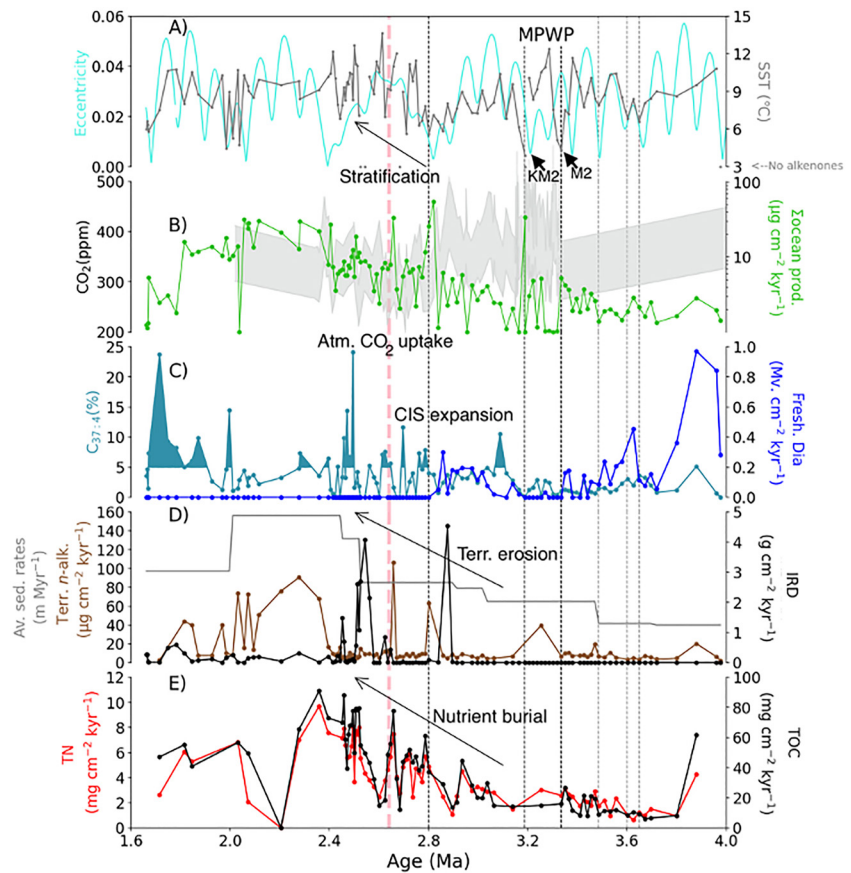


Figure 5. The development of the North Pacific stratification and the nitrogen and carbon cycling. (a) Earth's eccentricity reconstruction (light blue; Berger & Loutre, 1999) and U^{K}_{37} sea surface temperatures (SST) ($^{\circ}\text{C}$) at Site U1417 (gray; Sánchez-Montes et al., 2019); (b) atmospheric CO_2 upper- and lower-end (ppm) estimates on the Caribbean Sea based on alkenone $\delta^{13}\text{C}$ (Site Ocean Drilling Program (ODP) 999A; Seki et al., 2010) and marine $\delta^{11}\text{B}$ (Site ODP 999; Martínez-Botí et al., 2015; de la Vega et al., 2020) (gray) and sum of ocean productivity proxies (alkenone, brassicasterol and aquatic n -alkane mass accumulation rates (MAR), $\mu\text{g cm}^{-2} \text{kyr}^{-1}$, light green, in log scale); (c) $C_{37:4}$ (%) as a record of meltwater inputs (turquoise, Sánchez-Montes et al., 2019) and freshwater diatom MAR (blue, million valves $\text{cm}^{-2} \text{kyr}^{-1}$, blue); (d) terrigenous (brown) n -alkane MAR ($\mu\text{g cm}^{-2} \text{kyr}^{-1}$), average sedimentation rates at U1417 (grey, m Myr^{-1} ; Sánchez-Montes et al., 2019) and IRD MAR (black, $\text{g cm}^{-2} \text{kyr}^{-1}$; Sánchez-Montes et al., 2019) and (e) total nitrogen (TN; red) and total organic carbon (TOC; black) MAR ($\text{mg cm}^{-2} \text{kyr}^{-1}$) at Site U1417 versus age in million years before present (Ma; Sánchez-Montes et al., 2019). Gray dashed vertical lines indicate the timing of the Gi4, Gi2 and disappearance of silicoflagellates (see Figure 3). Black dashed lines indicate the timing of the M2, KM2, which capulate the Mid Piacenzian Warm Period (MPWP), and the start of the intensification of the CIS (iCIS). Pink vertical dashed line indicates the maximum extension of the Cordilleran Ice Sheet (CIS) at the lower Klondike Valley, Yukon interior (2.64 Ma; Hidy et al., 2013). Black arrows highlight the tendency of the proxies at key intervals.

overall decrease in freshwater diatoms (Figure 4b). Progressively increasing $\delta^{13}\text{C}$ but decreasing $\delta^{15}\text{N}$ across the late Pliocene suggests a limited carbon but abundant bioavailable nitrogen pool for phytoplankton consumption (Figure 2c). A reduced ocean mixing/more stratified water column, caused by slow ocean circulation or reduced gravity flow movement, would limit the atmosphere-ocean ^{12}C exchange and increase bacterial nitrogen fixation (Galbraith et al., 2004).

The continuous presence of benthic diatoms suggests that downslope transport towards Site U1417 still occurred during the late Pliocene but was reduced. The decrease in river transport could reflect an increasingly glaciated landscape, as suggested in Sánchez-Montes et al. (2020), which is supported by higher sedimentation rates (Figure 5d; Gulick et al., 2015). Reduced downwelling is suggested by decreased silica preservation and increased organic matter preservation. Further, the LNHC region in the GOA reduced in extent due to a higher macronutrient availability and allowed the expansion of marine pelagic communities across a range of producers (including

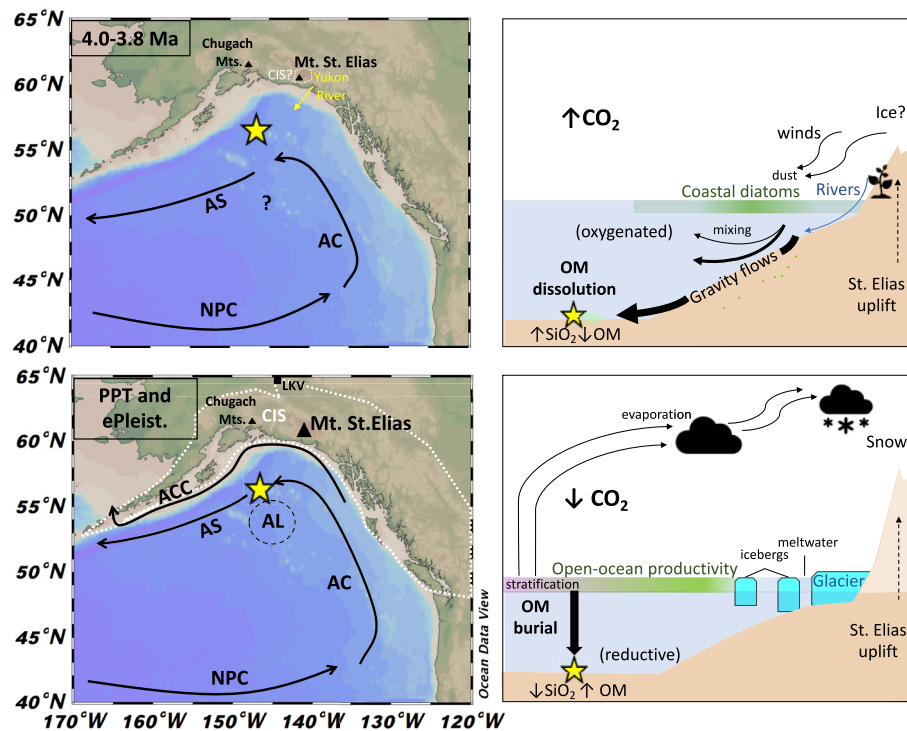


Figure 6. Schematic overview of the Plio-Pleistocene changes in the GOA's atmosphere and ocean circulation. Left) Schematic circulation over a modern map of the Gulf of Alaska (GOA) with similar labels as in Figure 1 (Ocean Data View; Schlitzer, 2016) and right) Alaskan coast to Site U1417 transect simplifying the water column characteristics discussed in the text during the top) early Pliocene (4.0–3.8 Ma) and bottom) the Plio-Pleistocene Transition (PPT) and early Pleistocene (ePleist). The top left panel indicates a weaker and possibly different ocean circulation than at present, and the Yukon River Basin runoff during the Pliocene (yellow arrow; Duk-Rodkin et al., 2004) and possible Cordilleran Ice Sheet (CIS) extension (interpreted from Enkelmann et al., 2015; white dashed line) and smaller St. Elias Mountain altitude (interpreted from Enkelmann et al., 2015; black triangles). The bottom left panel indicates the CIS Pliocene-early Pleistocene maximum extension (Duk-Rodkin et al., 2004; Hidy et al., 2013; white dashed line; LKV = Lower Klondike Valley) and higher Mt. St. Elias altitude (>2,000 m, Duk-Rodkin et al., 2004, bigger black triangle).

diatoms and coccolithophores, Figures 3d and 4b) and increased the overall ocean diversity (Figure 3b). In addition, the less mixed water column would have favored bacterial nitrogen fixation (Galbraith et al., 2004), phytoplankton nitrogen consumption and phytoplankton nitrogen burial (Figure 4d).

As the glaciation progressed during the late Pliocene, there is evidence of tectonic uplift and glaciations causing changes in the Alaskan landscape such as a shift in the Yukon River flow, from originally southward direction to the GOA to flow westward to the Bering Sea (Duk-Rodkin et al., 2004), which would have reduced riverine terrestrial and freshwater input to the GOA. Similarly, reversal of the Bering Strait throughflow from southward to northward at 3.6 Ma (Horikawa et al., 2015) away from the North Pacific to the Arctic Ocean, may also have impacted the ocean circulation in the GOA. The resulting enhanced organic matter MAR from reduced river runoff and decrease in strength of ocean currents in the GOA could reflect improved preservation resulting from a more stratified water column.

The Mid Piacenzian Warm Period (MPWP) (3.33–3.19 Ma) is noted separately here as it has several specific characteristics which are different from the rest of the Pliocene at Site U1417. Although there is a sharp reduction in diatom MAR (3.25–3.19 Ma; Figure 4a) elevated marine export productivity is indicated by high abundances of pelagic diatom species (with an average of 88%, Figure 3d) accompanied by peaks in brassicasterol (Figure 4a), alkenone (Figure 4b) and aquatic *n*-alkane (Figure 4c) MAR, alongside peaks in Ba/Al (330–350 ppm %⁻¹) and CaCO₃ (<2%) at Site U1417 (Jaeger et al., 2014; Zindorf et al., 2019). The higher susceptibility of brassicasterol than alkenones to degradation (Gaskell & Eglinton, 1974.; Wakeham et al., 2002) suggest a combined favouring of water chemistry and nutrient regime for brassicasterol producers (diatoms) to the detriment of alkenone producers (haptophyte). The reduced diatom diversity and shift to increasingly open ocean productivity

conditions, dominated by pelagic high productivity environments, is consistent with the reduction of diatom biodiversity in other marine habitats (Figure 5b) (Nakov et al., 2019).

The driver(s) for the enhanced MPWP marine production at Site U1417 could reflect enhanced nutrient supply to the center of the Alaskan gyre as productivity gradients relax during warmer intervals (Figure 1) and/or improved preservation of the productivity proxies. There is a sharp reduction in benthic and coastal high productivity diatoms during the MPWP since the marine isotope stage M2, suggesting that gravity flows decreased, which may have been aided by a decrease in riverine inputs due to the expansion of mountain glaciation in Alaska (Horikawa et al., 2015; Sánchez-Montes et al., 2020). Peaks in terrestrial *n*-alkane MAR show that erosion and transport of terrestrial material to the site was still occurring, potentially by wind and/or glaciers if riverine inputs were reduced (e.g., Müller et al., 2018; Sánchez-Montes et al., 2020). These terrestrial inputs would likely still have provided a source of terrestrial iron. The general increase in ocean productivity (Figure 5b) during colder periods of the MPWP suggests increased atmosphere and ocean circulation and increased deep nutrient availability to the photic zone of the GOA under a HNLC region. Stratification during warmer periods of the MPWP would have been achieved by ice melting and increased ocean heat absorbance (e.g., Behera et al., 2021) while the MPWP poleward shift of the westerly winds might have been able to occasionally break the stratification in the GOA (Abell et al., 2021).

The overall sluggish circulation during the late Pliocene may suggest an ocean circulation reorganization in the GOA after the northward shift of the Yukon River outlet and Bering Strait throughflow. An interesting increase in pelagic warm water productivity (up to 45% of diatoms) might shed some light on the origin of the first $C_{37:4}$ peak above 5% in the GOA at 3.0 Ma, interpreted as the first evidence of glacier tidewater freshwater runoff in the GOA since 4.0 Ma (Sánchez-Montes et al., 2020). This could indicate that ice (i.e., tidewater glaciers) might have developed in the coastal GOA during the MPWP, the terminus of which might then have been melted by the northward advection of warm Pacific waters, such as the NPC (Figure 1). The injection of warm waters from lower latitude North Pacific to the GOA (shown by pelagic warm diatoms) and an increase in coastal moderate productivity diatoms seem to anticipate blooms in the gyre diatom communities (peaks in pelagic high productivity diatoms) characterising the transitional diatom communities during the late Pliocene. The new oceanography and reduction of freshwater input to the GOA allowed the Alaskan gyre to bring warm NPC waters to Site U1417. It might be that the new ocean configuration in the GOA with higher influence from lower latitudes during the late Pliocene allowed the rapid expansion of the CIS (Sánchez-Montes et al., 2020).

5.3. The Late Pliocene – Early Pleistocene (2.8–1.66 Ma): Increase in Organic Matter Export

The change from higher siliceous to higher organic matter productivity export, first observed in our record during the MPWP, becomes a permanent characteristic during the PPT and early Pleistocene (2.8–1.66 Ma; Figures 4a and 4b). The dominant pelagic contribution from diatoms to the productivity export since 2.8 Ma suggests that the alkenone MAR indicates total productivity export (Raja & Rosell-Melé, 2021) where the productivity was higher in central GOA and the productivity gradient shifted toward the coast (Figure 1). From 2.8 Ma, diatoms almost completely disappear from the record and TOC, TN and biomarkers increase more rapidly (Figure 4). Concentrations in terrestrial *n*-alkanes also increase but also become more variable, suggesting a mixture of transport mechanisms at play, for example, wind and glacial runoff (Figure 4d). The synchronous response of increasing terrigenous and aquatic *n*-alkanes seems to reflect ocean fertilisation through wind and/or glacial runoff-derived nutrients (Figures 4c and Figure 5c and 5d).

We propose that the increase in pelagic productivity from 2.8 Ma occurred under a strong Alaska gyre fueled by an Aleutian Low (AL) centered in the GOA (Sancetta & Silvestri, 1986) and highly functioning ocean-ice-climate linkages (Sánchez-Montes et al., 2020) which favored ocean fertilisation (Figure 6). Frequent glacial meltwater influence in the GOA is supported by peaks in $C_{37:4}$ above 5% after 2.8 Ma (Sánchez-Montes et al., 2020, Figure 5c), where sea-ice (Wang et al., 2021) at Site U1417's climatic setting likely played a minor role. A stratified and warmer water column (Figures 5a and 5c) could suggest a decrease in oxygen availability in the surface ocean and a shallower remineralization depth that favored the carbon pump (Crichton et al., 2021). Warm intervals of the GOA have previously been linked to a decrease in dissolved oxygen (Barron et al., 2009; Galbraith et al., 2004; Zindorf et al., 2020). Since the late Pliocene until 2.4 Ma, the $\delta^{13}C$ and $\delta^{15}N$ display a variable but an overall decreasing trend, suggesting a progressively larger pool of carbon and bioavailable nitrogen feeding the marine phytoplankton. The increase in organic nitrogen during 2.8–2.4 Ma suggests a slow ocean circulation

and an overall stratified water column (Galbraith et al., 2004), storing nutrients in the deeper ocean, where nitrogen could become bioavailable by increased nitrogen fixation and would become available to the surface with episodes of ocean mixing. During the early Pleistocene (2.4–1.66 Ma) the $\delta^{13}\text{C}$ remains low, however the $\delta^{15}\text{N}$ increases suggesting an increase in inorganic nitrogen supply (Figure 3c).

The higher alkenone and brassicasterol (haptophyte and diatoms) export suggests that the GOA iron abundance decreased during the late Pliocene-early Pleistocene similarly to during the MPWP and at modern times (Hinckley et al., 2009; Martin et al., 1991; Martin & Fitzwater, 1988). The marine productivity, controlled by the availability of nutrients accumulated in the deep GOA, is made available when increased wind speeds increased ocean mixing, interrupting an otherwise highly stratified water column configuration (peaks in alkenones and brassicasterol, Figures 4a and 4b; Abell et al., 2021; Sánchez-Montes et al., 2020). The highest TOC and TN of the record are found between 2.4 and 1.66 Ma suggesting the highest carbon and nitrogen deep ocean storage. However, TOC and TN show a slowly decreasing trend which, together with similar $\delta^{13}\text{C}$ and an increase in $\delta^{15}\text{N}$ from the previous interval (2.8–2.4 Ma), suggests a shift towards reducing organic carbon export to the deep sea, perhaps reflecting enhanced respiration in the water column and return of carbon to the atmosphere under an intensified ocean circulation (Galbraith et al., 2004). A better ventilated ocean is consistent with the frequent peaks in terrestrial *n*-alkanes attributed previously to strong winds, which could have promoted oxygenated conditions in the GOA, consistent with our observed decrease in brassicasterol preservation and increased diatom concentrations (although still very low, 0.04–0.4 Million valves $\text{cm}^{-2} \text{kyr}^{-1}$) (Figure 4). The increase of diatoms (2.0–1.66 Ma) supports the aeolian supply of terrestrial nutrients, possibly aided by glacial meltwater input. Upwelling centered in the GOA and ocean fertilization is a characteristic of the northeast Pacific at present under the influence of the AL atmospheric circulation and HNLC configuration.

During 2.4–2.0 Ma, the increase in alkenone MAR (Figures 4a and 4b) and the fragmentary brassicasterol record suggest a less stratified ocean column and increased upwelling conditions in the HNLC region. Intensified winds during 2.4–1.66 Ma (deduced from high terrestrial *n*-alkane concentrations) under the influence of the AL and increased deep ocean mixing due to increased gyre circulation might have been responsible for the increases in terrestrial input and deep nutrient availability in the photic zone, respectively, corresponding to a HNLC region. The increase in nutrient availability resulted in a higher marine productivity export and high carbon and nitrogen deep storage (high TN, TOC; Figure 5e) which suggests a still strongly reductive ocean interior.

5.4. Implications for Ocean Circulation and CO_2 Storage in the GOA During the CIS Development

We have outlined several scenarios of changing Pliocene and early Pleistocene productivity in the GOA, as well as changes in likely nutrient sources. The biogeochemical changes in the water column described at Site U1417 follow an eccentricity-driven ~ 400 kyr cyclicity (Figure 3). Although the patterns are complex, we note that low eccentricity periods can be linked to surface ocean cooling and changes in the CIS extent (Figure 5). We suggest here that this, in turn, resulted in impacts on nutrients and productivity offshore linked to changes in the AC and the AL (Barron, 1998; Sancetta & Silvestri, 1986). We propose that eccentricity minima and cooler periods on land triggered an increased glaciation and changed the regional oceanography of the GOA via internal feedback mechanisms. For example, the disappearance of silicoflagellates (3.48 Ma), the reduced diatom productivity export (M2 and KM2) and the disappearance of diatoms (2.8 Ma) all mark the Pliocene ~ 400 kyr eccentricity cycles of silica dissolution under increased ocean reductive conditions linked to a shift toward increased gyre circulation.

The 100 kyr cycles of lower amplitude eccentricity changes can be linked to a slightly more active gyre circulation and are also reflected in relatively cool periods such as the Gi4 at 3.65 Ma and Gi2 at 3.60 Ma. Stage Gi4 impacted productivity export by decreasing the terrestrial freshwater diatom and increasing marine OM inputs to Site U1417. Peaks in alkenone MAR at Site U1417 mark the 400 kyr and some 100 kyr low eccentricity events and could be attributable to a higher biological pump during cooler climate (Boscolo-Galazzo et al., 2021; Crichton et al., 2021, Figure 4b). These low eccentricity conditions intensified overall during the CIS expansion at 2.8 Ma (Figure 5), where the Alaskan gyre became more active driving pelagic productivity at the center of the GOA. Decrease in diatom and increases in pelagic high productivity at the center of the Alaskan gyre suggests a steep productivity gradient shifted toward the coastal region (Figures 4 and 5) (Barron, 1998). Productivity peaks in the subarctic Pacific have been associated with lower dissolved oxygen under warmer climate (Barron et al., 2009; Knudson et al., 2021), which suggests a more reductive ocean during the PPT and an increase in carbon burial

efficiency (Lopes et al., 2015). Lower productivity during warmer sea surface temperatures (SSTs), with a stratified ocean and increased atmospheric oxygen, has also been suggested due to a higher carbon remineralization in the water column and lower C pump (Boscolo-Galazzo et al., 2021; Crichton et al., 2021; Fakhraee et al., 2020; Komar & Zeebe, 2021). However, in the northeast Pacific, ecosystem and sea-floor controls have been identified as playing a bigger role than SST to increase carbon export despite lower productivity (Lopes et al., 2015). In addition, under a warmer climate and more stratified ocean, productivity export has been suggested to increase due to an increase in carbon remineralization in the upper ocean resulting in increase in productivity, whereas the carbon pump remains largely similar before and after warming (Crichton et al., 2021). SSTs increase $\sim 1^\circ\text{C}$ at Site U1417 during the early Pleistocene in comparison with the late Pliocene (Sánchez-Montes et al., 2020). An SST increase of 0.6°C is estimated to reduce the particulate organic carbon at a 1 km water column depth by 5% (Crichton et al., 2021). Carbon remineralization at 4 km deep (Site U1417) is therefore likely to have contributed minimally to decrease C export across the Plio-Pleistocene, where other sites in the northeast Pacific register lower SSTs (Sánchez-Montes et al., 2020). As a result, we do not think that changes in organic matter remineralization in response to changing ocean temperatures can account for the shift in MAR we identify here, leaving a change in export production as the most likely driver of the changes we observe. During the CIS retreat at 1.9 Ma, offshore productivity is high as well as the transport of coastal productivity diatoms returns to Site U1417 suggesting an increase in iron delivered to the GOA (Costa et al., 2016) and a return to slightly more oxygenated conditions.

Site U1417 sits in the Surveyor Fan while Ocean Drilling Program (ODP) 887 sits in the Aleutian Abyssal Plain (Rea & Snoeckx, 1995). While we note an apparent higher terrigenous input at ODP 887 than U1417 across the Pliocene and early Pleistocene (Figure 7), these records need to be considered to reflect different environmental proxies (coarse and fine mineral clasts vs. long-chain n-alkanes, respectively) and settings. Sedimentation rates are higher at Site U1417 than ODP 887 across the Pliocene and early Pleistocene (Jaeger et al., 2014; Rea & Snoeckx, 1995) suggesting higher terrigenous inputs to Site U1417 than ODP 887, which is explained by proximity to the CIS (ODP 887 is located 200 km southwest of U1417, further away from the CIS; Figure 7). Site U1417 recorded similar biogenic silica MAR to ODP 887 (3,634-m water depth, Figure 7). Compared to other sites of the North and equatorial Pacific, Site U1417 and ODP 887 contain the lowest biogenic silica and alkenone MAR during the Pliocene-early Pleistocene (Figure 7). This could suggest a similar biogenic silica preservation across the east subarctic Pacific due to more oxygenated/reduced water column (Galbraith et al., 2004), where ODP 887, closer to the centre of the AL suffered larger variations in silica preservation than Site U1417 which is located under the AC (Figure 7). Comparing the subpolar gyre, which expands across Site U1417, ODP 887 and ODP 882, there is an order of magnitude higher biogenic silica MAR at ODP 882, under the influence of the Kamchatka Current in the west subarctic Pacific (3,244 m water depth) than in the GOA (Figure 7). The highest alkenone MAR are recorded at Site 1012, under the influence of the California Current (1,772 m water depth, Figure 7), followed by ODP 846 under the Peru Current and close to the Equatorial Undercurrent (3,307 water depth, Figure 7). According to these patterns, the sites located in shallower water depths exhibited the highest productivity MAR, which suggests better preservation but could also suggest that shallower water columns were more easily mixed or had greater terrestrial nutrient supply to trigger productivity blooms.

However, as noted for Site U1417, the PPT development of the CIS and the NHG more generally affected the preservation of siliceous and organic matter remains in the whole North Pacific, where biogenic silica decreases and organic matter increases (Figure 7). In addition, terrestrial inputs during the PPT increase, suggesting ocean fertilisation and an increase in marine productivity in the northeast and possibly the equatorial Pacific (Figure 7). In particular across 2.4–2.0 Ma, ocean fertilisation and productivity at the North Pacific Site U1417 and ODP 1012 are maximum during the increase in gyre circulation (e.g., Barron et al., 2002) and increase in AL and North Pacific High systems, which suggest an increase in the westerly wind strength (Abell et al., 2021). The east equatorial Pacific, however, shows a decrease in coccolithophore productivity probably explained by weaker trade winds at ODP 846 and disruptions in the Pacific Cold Tongue (Liu et al., 2019). From all regions represented in Figure 7, ODP 846 is the only region that cooled across the PPT (Sánchez-Montes et al., 2020), supporting weaker trade winds and a rapid switch from La Niña to El Niño-like conditions. The same northeast Pacific productivity and terrigenous input pattern observed for 2.4–2.0 Ma also appears during the MPWP, when a weaker east equatorial Pacific upwelling system suggests an expansion of the equatorial warm pool (Liu et al., 2019). The expansion of the equatorial warm pool also suggests a nutrient leakage of deep ocean nutrients (macronutrients) to northern latitudes and a drier Asian continent to increase in dust (micronutrients) from the Loess Plateau to

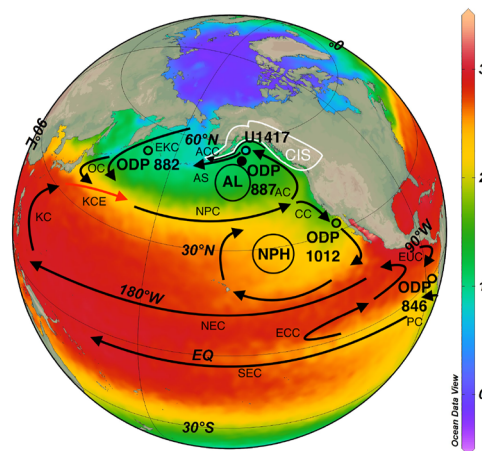
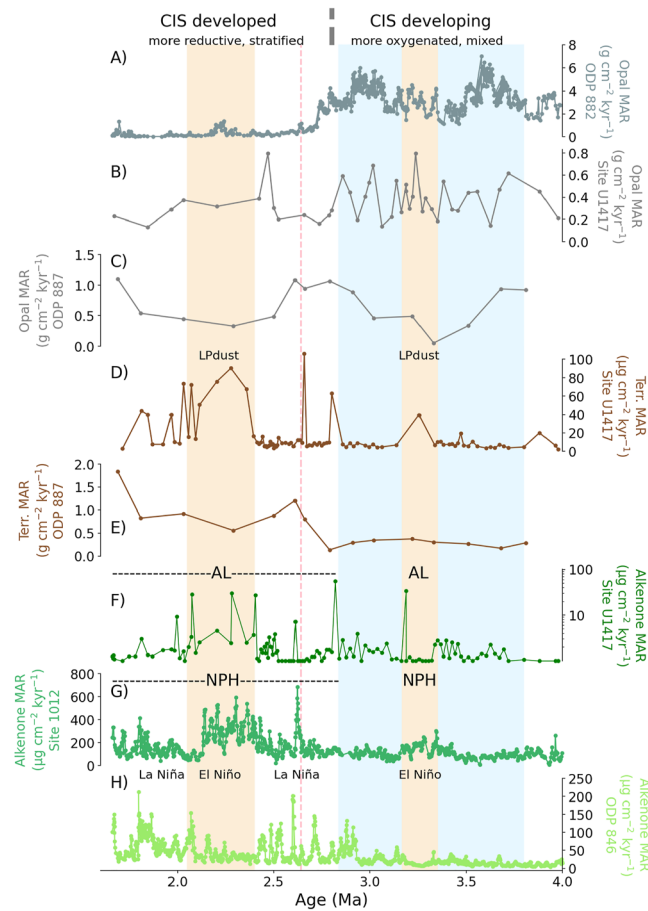


Figure 7.

the North Pacific (Abell et al., 2021), driving the highest sustained coccolithophore productivity between 2.4 and 2.0 Ma and the shift to open ocean productivity during the MPWP and HNLC conditions. The nutrient leakage from the equatorial to the North Pacific seems to have also played a role in the biogeochemistry changes observed at Site U1417 discussed above. Furthermore, these mechanisms aid a detachment from the aeolian and the riverine/glacial terrigenous *n*-alkane signal. The highest peaks in terrigenous *n*-alkanes at Site U1417 seem to be driven by an increase of terrigenous inputs from the Loess Plateau under a stronger atmospheric and ocean circulation (Abell et al., 2021), whereas the background (smaller) peaks seem to correlate with increase in riverine/glacial terrigenous inputs from the GOA (Figure 7d). Source studies of terrestrial input to Site U1417

during the PPT and early Pleistocene suggest similar to modern coastal detrital provenance of Alaskan coast and Asia (Rea, Basov, Krissek, & the Leg 145 Scientific Party, 1995; Rea, Basov, Scholl, & Allan, 1995; Horikawa et al., 2015) of the inorganic nitrogen and iron input to Site U1417 (Figure S1 in Supporting Information S1). The erosion of lithologies at lower altitudes as the glaciation progresses (Figure S1 in Supporting Information S1, Perry et al., 2009; Chapman et al., 2012) is consistent with more recent source interpretations in the GOA (Huber & Bahlburg, 2021).

In addition, the change in heat supply from the equator to the North Pacific due to oceanographic changes might have resulted in the CIS glaciation attempt during the M2 (De Schepper et al., 2013) and CIS build up across the 2.4–2.0 Ma (Site U1417 highest sedimentation rates, Figure 5d). The Kuroshio Extension characteristic microfossil tropical species (Lam & Leckie, 2020) and its increase at Site U1417 during stronger North Pacific gyre circulation (Gallagher et al., 2015) suggest the Kuroshio Extension influence in the GOA since the late Pliocene (Gallagher et al., 2015). The expanded storm track which characterizes modern El Niño (Joh et al., 2021), in addition to a the permanent negative Pacific Decadal Oscillation-like climate in the North Pacific across the Pliocene-early Pleistocene (Sánchez-Montes et al., 2020) and mountain building (Enkelmann et al., 2015) would increase ice accumulation on land under lower atmospheric CO₂ concentrations (Figure 5a).

The eccentricity and biogeochemical changes observed in the GOA are observable in the North Pacific, at least at the 400 kyr cycles with some other cycles that are marked by eccentricity minima at 3.8, 3.3, 3.2, 2.8, 2.4 and 2.0 Ma, where the subpolar gyre has been suggested to be the driver of changes in the subtropical Pacific gyre (Sancetta & Silvestri, 1986). Despite higher biogenic silica concentrations than Site U1417 before the PPT, ODP 882 and ODP 887 biogenic silica MAR decrease to comparable concentrations than Site U1417 after the PPT resulting in an average homogeneous biogenic silica MAR of 0.4 g cm⁻² kyr⁻¹ across east and west subarctic Pacific (Figure 7). The southward component of the Bering Sea (Horikawa et al., 2015) and the Yukon River flow during the early Pliocene (Duk-Rodkin et al., 2004), together with the productivity characteristics of the subarctic Pacific suggests that the early Pliocene circulation in the North Pacific was different compared to modern, probably caused by a different topography due to ongoing tectonic changes in coastal Alaska (Enkelmann et al., 2015). However, during the PPT, the west subarctic Pacific and the Alaska gyre unified under a HNLC region during the ocean reorganization across the late Pliocene and water column stratification during the intensification of the CIS (iCIS). This suggests a closer cycling of ocean currents between east and west Pacific, with the AS traveling westward in a subpolar gyre similar to present. We further suggest that the new ocean configuration of strong Alaska Gyre and increased ACC transport from the GOA through the Bering Sea toward the Arctic (Horikawa et al., 2015) may have contributed to freshening in the Arctic Ocean and sea-ice formation (Matthiessen et al., 2009).

Unlike the rest of the Pacific sites in Figure 7, the development of the subarctic Pacific HNLC is a key region because of the increases in phytoplankton productivity and preservation associated with the development of the CIS and water column stratification and the impacts on the C budget via atmospheric CO₂ drawdown. This is especially important considering that before the iCIS and ocean stratification, the subarctic Pacific's effective respiration of organic matter would have contributed to maintaining the high Pliocene CO₂ concentrations via ocean carbon degassing (Figure 6). The subarctic Pacific HNLC region is subject to availability of micronutrients to the photic zone (Crichton et al., 2021) and therefore, the GOA closer to the CIS (in particular Site U1417,

Figure 7. Productivity and ocean circulation in the north Pacific. Upper panel: (a) ODP 882 biogenic silica mass accumulation rates (MAR) (g cm⁻² kyr⁻¹) located in the subarctic west (Haug et al., 1999), (b) Site U1417 biogenic silica MAR (g cm⁻² kyr⁻¹), (c) ODP 887 biogenic silica MAR (g cm⁻² kyr⁻¹), located 200 km southwest of U1417 (Rea & Snoeckx, 1995), (d) Site U1417 terrigenous *n*-alkane MAR (μg cm⁻² kyr⁻¹), (e) ODP 887 total terrigenous MAR (g cm⁻² kyr⁻¹) (Rea & Snoeckx, 1995), (f) Site U1417 alkenone MAR (μg cm⁻² kyr⁻¹), (g) Site U1012 alkenone MAR (μg cm⁻² kyr⁻¹), located in the east Cortez Basin, 100 km southwest of San Diego (Liu et al., 2008) and (h) ODP 846 alkenone MAR (μg cm⁻² kyr⁻¹), in the equatorial east Pacific (Liu & Herbert, 2004) where references to La Niña and El Niño refer to La Niña and El Niño-like conditions. Blue vertical shadings indicate the transitional water columns across more oxygenated (4.0–3.8 Ma) to more reductive (3.3–3.2 Ma, Mid Piacenzian Warm Period (MPWP)) and from the more reductive MPWP through more oxygenated (3.2–2.82 Ma) to more reductive (2.8–1.66 Ma). Pink vertical dashed line indicates the maximum extension of the Cordilleran Ice Sheet (CIS) at the lower Klondike Valley, Yukon interior (2.64 Ma; Hidy et al., 2013). Orange shadings indicate higher terrestrial *n*-alkanes from the Loess Plateau (LPdust) and higher alkenone MAR at Site U1417 and Site 1012, associated with El Niño-like conditions. Lower panel: Pacific globe view with modern ocean circulation (Ocean Data View; Schlitzer, 2016), summer SSTs (September 1955–2013, NOAA WOA13; Locarnini et al., 2013) and location of drilling sites shown in the upper panel circle-colored with the early Pleistocene SST average, which depict North Pacific SST gradients similarly to the negative Pacific Decadal Oscillation (PDO) (discussed in Sánchez-Montes et al., 2020; black filling at ODP 887 indicates no data). PC = Peru Current, SEC = South Equatorial Current, ECC = Equatorial Countercurrent, EUC = Equatorial Undercurrent, NEC = North Equatorial Current, EKC = East Kamchatka Current, OC = Oyashio Current, KC = Kuroshio Current, KCE = Kuroshio Current Extension, NPC = North Pacific Current, AC = Alaska Current, ACC = Alaska Coastal Current, AS = Alaska Stream and CC = California Current. CIS = Cordilleran Ice Sheet extent (early Pleistocene maximum extension, Duk-Rodkin et al., 2004; Hidy et al., 2013; white line), AL = Aleutian Low and NPH = North Pacific High.

which registers sedimentation rates four times higher than ODP 887, Jaeger et al., 2014; Rea & Snoeckx, 1993) plays a key role in C fixation and burial. Considering the GOA defined as the area contained within a line across the Kodiak Island and the Dixon Entrance (USGS, 1981), the Surveyor Fan extends across two thirds of the GOA, the other one third is occupied by the Baranoff Fan and ODP887, in the Aleutian Abyssal Plain, is excluded (Rea & Snoeckx, 1993). The Surveyor and Baranoff Fans share similar climatic and tectonic history, where they transitioned from riverine toward higher glacial inputs through the Pleistocene, however the sediment provenance of the Baranoff Fan in the Coast Mountains (Walton et al., 2014) is different to the Surveyor Fan from the St. Elias Mountains (Enkelmann et al., 2015) and there is a lack of understanding of the area to date. Thus, based on the Surveyor Fan alone and assuming similar sedimentation rates and marine productivity responses to the climate changes across the fan, increases in TOC MAR at Site U1417 across the PPT results to an estimated 404 ± 23 Pg carbon export increase in the Surveyor Fan during the iCIS and early Pleistocene in comparison to the rest of the Pliocene. The increase in organic carbon burial of the order of $186 \pm 20\%$ in the Surveyor Fan occurred during a period of $13 \pm 2\%$ decrease in the global atmospheric CO_2 across the iCIS and early Pleistocene (de la Vega et al., 2020). This might suggest that despite the GOA is a small area, the increase in the sediment rates and organic matter burial across the early Pleistocene could have contributed to the global atmospheric CO_2 reduction. However, these numbers are indicative only, and more research is needed to quantify the maximum and minimum extent of carbon burial more accurately during the Plio-Pleistocene transition. Both elevated productivity and better organic matter preservation could have been important for increasing deep ocean and sediment storage of organic matter, and potentially drawing down atmospheric CO_2 and cooling the climate (e.g., Burdige, 2007) under short (orbital) time scales (e.g., during low eccentricity intervals in the MPWP; de la Vega et al., 2020, Figure 5b), and longer time scales (e.g., across the PPT). In addition, high marine diversity during the late Pliocene might have slowly contributed to atmospheric CO_2 drawdown as suggested for the present day (Palevsky et al., 2013). Globally, the atmospheric CO_2 decreased about 100 ppm during the PPT (Figure 5b), where 40% of the modern decadal atmospheric CO_2 variability has been attributed to ocean forcing (DeVries et al., 2019). Similarly as what we find in the GOA during the PPT, carbon sinking at modern is accelerating in the Pacific (Carter et al., 2019). Further work is needed to estimate the GOA's contribution to global atmospheric CO_2 decrease during the Pliocene and Pleistocene.

6. Conclusions

The Pliocene and early Pleistocene productivity at Site U1417 is characterized by a decrease in siliceous microfossil export from coastal habitats and an increase in pelagic organic matter productivity. We attribute this change to a biogeochemical shift from (i) an oxygenated, high micro-nutrient availability but low nitrogen bioavailability (low nutrient high chlorophyll, LNHC region), to a (ii) reductive deep GOA, with restricted macro and micro-nutrients but increased nitrogen bioavailability (high-nutrient-low-chlorophyll, HNLC region), during the Plio-Pleistocene transition (PPT). We conclude that both tectonic uplift in the St. Elias mountains since the Pliocene and short-lived low eccentricity cycles increased the CIS glaciation and altered atmospheric and ocean circulation patterns, ocean biogeochemistry, and marine productivity. The stronger eccentricity cycles (~400 kyr) marked glacial events, with associated peaks in marine productivity export which could have drawn down CO_2 from the atmosphere during, for example, the KM2 at 3.2 Ma, at 2.8 Ma, 2.4 Ma and 2.0 Ma. In contrast, during the shorter (100 kyr) higher eccentricity period glacials, climate feedback mechanisms of increased glaciation on land, decrease riverine and terrestrial nutrient inputs to the GOA derived in enhanced HNLC conditions and increased reductive conditions in the GOA. Over longer time scales (PPT), the GOA is potentially an important region due to the variability and, crucially, the increase in ocean fertilisation taking place. Changes in bottom water conditions, in particular trends to more reductive conditions can potentially help to account for increasing glaciation in Alaska, potentially having an impact on decreasing atmospheric CO_2 concentrations and contributing to cooling the climate.

Data Availability Statement

The new datasets in this article are available at Pangaea (Sánchez-Montes et al., 2021).

Acknowledgments

We would like to acknowledge the International Ocean Discovery Program U.S. Implementing Organization (IODP-USIO) and the captain and crew of the D/V *Joides Resolution*. This work was supported by funding from Van Mildert College and the Durham Doctorate Scholarship (MLSM), the NERC-IODP (grant no. NE/L002426/1, ELM), the German Research Foundation (Grant Nos. MU3670/1-2, JM) and the Helmholtz Association (Grant Nos. VH-NG-1101, JM). The authors declare no conflict of interest. We are grateful for the discussion with George Swann and Antoni Rosell-Melé on an earlier version of this manuscript. We thank Coralie Zorzi for discussions of pollen sources on this site. We thank Martin West, Amanda Hayton, and Kathryn Melvin for assistance with the GCMS analyses. We extend our thanks to P&P editor Matthew Huber and associate editor Yige Zhang, John Barron and reviewers 2 and 3 for providing comments that improved our manuscript.

References

- Abell, J. T., Winckler, G., Anderson, R. F., & Herbert, T. D. (2021). Poleward and weakened westerlies during Pliocene warmth. *Nature*, 589(7840), 70–75. <https://doi.org/10.1038/s41586-020-03062-1>
- Addison, J. A., Finney, B. P., Dean, W. E., Davies, M. H., Mix, A. C., Stoner, J. S., & Jaeger, J. M. (2012). Productivity and sedimentary $d^{15}N$ variability for the last 17, 000 years along the northern Gulf of Alaska continental slope. *Paleoceanography*, 27(1), PA1206. <https://doi.org/10.1029/2011pa002161>
- Ausin, B., Bruni, E., Haghypour, N., Welte, C., Bernasconi, S. M., & Eglinton, T. I. (2021). Controls on the abundance, provenance and age of organic carbon buried in continental margin sediments. *Earth and Planetary Science Letters*, 558, 116759. <https://doi.org/10.1016/j.epsl.2021.116759>
- Ausin, B., Magill, C., Haghypour, N., Fernández, Á., Wacker, L., Hodell, D., et al. (2019). Coherent multiproxy signals in marine sediments: Implications for high-resolution paleoclimate reconstruction. *Earth and Planetary Science Letters*, 515, 38–46. <https://doi.org/10.1016/j.epsl.2019.03.003>
- Barron, J. A. (1998). Late Neogene changes in diatom sedimentation in the North Pacific. *Journal of Asian Earth Sciences*, 16(1), 85–95. [https://doi.org/10.1016/S0743-9547\(97\)00046-9](https://doi.org/10.1016/S0743-9547(97)00046-9)
- Barron, J. A., Bukry, D., Dean, W. E., Addison, J. A., & Finney, B. (2009). Paleoceanography of the Gulf of Alaska during the past 15, 000 years: Results from diatoms, silicoflagellates, and geochemistry. *Marine Micropaleontology*, 72(3–4), 176–195. <https://doi.org/10.1016/j.marmicro.2009.04.006>
- Barron, J. A., Lyle, M., & Koizumi, I. (2002). Late Miocene and early Pliocene biosiliceous sedimentation along the California margin. *Revista Mexicana de Ciencias Geológicas*, 19(003), 161–169.
- Behera, P., Tiwari, M., & Knies, J. (2021). Enhanced Arctic stratification in a warming scenario: Evidence from the Mid Pliocene warm period. *Paleoceanography and Paleoclimatology*, 36(6). <https://doi.org/10.1029/2020pa004182>
- Berger, A., & Loutre, M.-F. (1999). Parameters of the Earth's orbit for the last 5 Million years in 1 kyr resolution. *PANGAEA*. <https://doi.org/10.1594/PANGAEA.56040>
- Boscolo-Galazzo, F., Crichton, K. A., Ridgwell, A., Mawbey, E. M., Wade, B. S., & Pearson, P. N. (2021). Temperature controls carbon cycling and biological evolution in the ocean twilight zone. *Science*, 371(6534), 1148–1152. <https://doi.org/10.1126/science.abb6643>
- Bourbonniere, R. A., & Meyers, P. A. (1996). Sedimentary geolipid records of historical changes in the watersheds and productivities of Lakes Ontario and Erie. *Limnology & Oceanography*, 41(2), 352–359. <https://doi.org/10.4319/lo.1996.41.2.0352>
- Boyer, T. P., Antonov, J. I., Baranova, O. K., Coleman, C., Garcia, H. E., Grodsky, A., et al. (2013). World Ocean Database 2013, NOAA Atlas NESDIS 72. In S. Levitus (Ed.), *A. Mishonov, technical* (p. 209). Silver Spring. <https://doi.org/10.7289/V5NZ85MT>
- Burdige, D. J. (2005). Burial of terrestrial organic matter in marine sediments: A re-assessment. *Global Biogeochemical Cycles*, 19(4), GB4011. <https://doi.org/10.1029/2004GB002368>
- Burdige, D. J. (2007). Preservation of organic matter in marine sediments: Controls, mechanisms, and an imbalance in sediment organic carbon budgets? *Chemical Reviews*, 107(2), 467–485. <https://doi.org/10.1021/cr050347q>
- Carter, B. R., Feely, R. A., Wanninkhof, R., Kouketsu, S., Sonnerup, R. E., Pardo, P. C., et al. (2019). Pacific anthropogenic carbon between 1991 and 2017. *Global Biogeochemical Cycles*, 33(5), 597–617. <https://doi.org/10.1029/2018GB006154>
- Chapman, J. B., Pavlis, T. L., Bruhn, R. L., Worthington, L. L., Gulick, S. P. S., & Berger, A. L. (2012). Structural relationships in the eastern syntaxis of the St. Elias orogen, Alaska. *Geosphere*, 8(1), 105–126. <https://doi.org/10.1130/GES00677.1>
- Cortese, G., Gersonde, R., Hillenbrand, C.-D., & Kuhn, G. (2004). Opal sedimentation shifts in the World Ocean over the last 15 Myr. *Earth and Planetary Science Letters*, 224(3–4), 509–527. <https://doi.org/10.1016/j.epsl.2004.05.035>
- Costa, K., McManus, J., Anderson, R., Ren, H., Sigman, D., Winckler, G., et al. (2016). No iron fertilization in the equatorial Pacific Ocean during the last ice age. *Nature*, 529(7587), 519–522. <https://doi.org/10.1038/nature16453>
- Crichton, K. A., Wilson, J. D., Ridgwell, A., & Pearson, P. N. (2021). Calibration of temperature-dependent ocean microbial processes in the cGENIE.muffin (v0.9.13) Earth system model. *Geoscientific Model Development*, 14(1), 125–149. <https://doi.org/10.5194/gmd-14-125-2021>
- Crosta, X., Romero, O. E., Ther, O., & Schneider, R. R. (2012). Climatically-controlled siliceous productivity in the eastern Gulf of Guinea during the last 40 000 yr. *Climate of the Past*, 8(2), 415–431. <https://doi.org/10.5194/cp-8-415-2012>
- Crusius, J., Schroth, A. W., Gassó, S., Moy, C. M., Levy, R. C., & Gatica, M. (2011). Glacial flour dust storms in the Gulf of Alaska: Hydrologic and meteorological controls and their importance as a source of bioavailable iron. *Geophysical Research Letters*, 38(6), L06602. <https://doi.org/10.1029/2010GL046573>
- Crusius, J., Schroth, A. W., Resing, J. A., Cullen, J., & Campbell, R. W. (2017). Seasonal and spatial variabilities in northern Gulf of Alaska surface water iron concentrations driven by shelf sediment resuspension, glacial meltwater, a Yakutat eddy, and dust. *Global Biogeochemical Cycles*, 31(6), 942–960. <https://doi.org/10.1002/2016gb005493>
- de la Vega, E., Chalk, T. B., Wilson, P. A., Bysani, R. P., & Foster, G. L. (2020). Atmospheric CO₂ during the mid-piacenzian Warm Period and the M2 glaciation. *Scientific Reports*, 10(1), 11002. <https://doi.org/10.1038/s41598-020-67154-8>
- De Schepper, S., Groeneveld, J., Naafs, B. D., Van Renterghem, C., Hennissen, J., Head, M. J., et al. (2013). Northern Hemisphere glaciation during the globally warm early late Pliocene. *PLoS One*, 8(12), 1–15. <https://doi.org/10.1371/journal.pone.0081508>
- DeVries, T., Le Quéré, C., Andrews, O., Berthet, S., Hauck, J., Ilyina, T., et al. (2019). Decadal trends in the ocean carbon sink. *Proceedings of the National Academy of Sciences of the United States of America*, 116(24), 11646–11651. <https://doi.org/10.1073/pnas.1900371116>
- Duk-Rodkin, A., Barendregt, R. W., Froese, D. G., Weber, F., Enkin, R., Smith, I. R., et al. (2004). Timing and extent of the Plio-Pleistocene glaciations in north-Western Canada and east-central Alaska. *Developments in Quaternary Science*, 2, 313–345.
- Enkelmann, E., Koons, P. O., Pavlis, T. L., Hallet, B., Barker, A., Elliott, J., et al. (2015). Cooperation among tectonic and surface processes in the St. Elias Range, Earth's highest coastal mountains. *Geophysical Research Letters*, 42(14), 5838–5846. <https://doi.org/10.1002/2015GL064727>
- Etourneau, J., Ehlert, C., Frank, M., Martinez, P., & Schneider, R. (2012). Contribution of changes in opal productivity and nutrient distribution in the coastal upwelling systems to Late Pliocene/Early Pleistocene climate cooling. *Climate of the Past*, 8(5), 1435–1445. <https://doi.org/10.5194/cp-8-1435-2012>
- Fakhraee, M., Planavsky, N. J., & Reinhard, C. T. (2020). The role of environmental factors in the long-term evolution of the marine biological pump. *Nature Geoscience*, 13(12), 812–816. <https://doi.org/10.1038/s41561-020-00660-6>
- Galbraith, E. D., Kienast, M., Pedersen, T. F., & Calvert, S. E. (2004). Glacial-interglacial modulation of the marine nitrogen cycle by high-latitude O₂ supply to the global thermocline. *Paleoceanography*, 19(4), PA4007. <https://doi.org/10.1029/2003PA001000>
- Gallagher, S. J., Kitamura, A., Iryu, Y., Itaki, K., Koizumi, I., & Hoiles, P. (2015). The Pliocene to recent history of the Kuroshio and Tsushima currents: A multi-proxy approach. *Progress in Earth and Planetary Science*, 2(1), 17. <https://doi.org/10.1186/s40645-015-0045-6>
- Gaskell, S. J., & Eglinton, G. (1974). Short-term diagenesis of sterols. In *Adv. Org. Geochem., proc. Int. Meet., 6th* (pp. 963–976).

- GEBCO Compilation Group (2020). GEBCO 2020 Grid. <https://doi.org/10.5285/a29c5465-b138-234d-e053-6c86abc040b9>
- Goad, L., & Withers, N. (1982). Identification of 27-nor-(24R)-24-methylcholesta-5, 22-dien-3 β -ol and brassicasterol as the major sterols of the marine dinoflagellate *Gymnodinium simplex*. *Lipids*, 17(12), 853–858. <https://doi.org/10.1007/bf02534578>
- Gulick, S. P. S., Jaeger, J. M., Mix, A. C., Asahi, H., Bahlburg, H., Belanger, C. L., et al. (2015). Mid-Pleistocene climate transition drives net mass loss from rapidly uplifting St. Elias Mountains, Alaska. *Proceedings of the National Academy of Sciences of the United States of America*, 112(49), 15042–15047. <https://doi.org/10.1073/pnas.1512549112>
- Hage, S., Cartigny, M. J. B., Sumner, E. J., Clare, M. A., Hughes Clarke, J. E., Talling, P. J., et al. (2019). Direct Monitoring reveals initiation of turbidity currents from extremely dilute river plumes. *Geophysical Research Letters*, 46(20), 11310–11320. <https://doi.org/10.1029/2019GL084526>
- Hage, S., Galy, V. V., Cartigny, M. J. B., Acikalin, S., Clare, M. A., Gröcke, D. R., et al. (2020). Efficient preservation of young terrestrial organic carbon in sandy turbidity-current deposits. *Geology*, 48(9), 882–887. <https://doi.org/10.1130/G47320.1>
- Han, J., & Calvin, M. (1969). Hydrocarbon distribution of algae and bacteria, and microbiological activity in sediments. *Proceedings of the National Academy of Sciences*, 64(2), 436–443. <https://doi.org/10.1073/pnas.64.2.436>
- Haug, G., Sigman, D., Tiedemann, R., Pedersen, T., & Sarnthein, M. (1999). Onset of permanent stratification in the subarctic Pacific Ocean. *Nature*, 401(6755), 779–782. <https://doi.org/10.1038/44550>
- Haug, G. H., Ganopolski, A., Sigman, D. M., Rosell-Melé, A., Swann, G. E. A., Tiedemann, R., et al. (2005). North Pacific seasonality and the glaciation of North America 2.7 million years ago. *Nature*, 433(7028), 821–825. <https://doi.org/10.1038/nature03332>
- Hedges, J. I., & Keil, R. G. (1995). Sedimentary organic matter preservation: An assessment and speculative synthesis. *Marine Chemistry*, 49(2–3), 81–115. [https://doi.org/10.1016/0304-4203\(95\)00008-F](https://doi.org/10.1016/0304-4203(95)00008-F)
- Herbert, T. D. (2001). Review of alkenone calibrations (culture, water column and sediments). *Geochemistry, Geophysics, Geosystems*, 2, 2000GC000055.
- Hidy, A. J., Gosse, J. C., Froese, D. G., Bond, J. D., & Rood, D. H. (2013). A latest Pliocene age for the earliest and most extensive Cordilleran Ice Sheet in northwestern Canada. *Quaternary Research*, 61, 77–84. <https://doi.org/10.1016/j.quascirev.2012.11.009>
- Hinckley, S., Coyle, K. O., Gibson, G., Hermann, A. J., & Dobbins, E. L. (2009). A biophysical NPZ model with iron for the Gulf of Alaska: Reproducing the differences between an oceanic HNLC ecosystem and a classical northern temperate shelf ecosystem. *Deep-Sea Research II*, 56(24), 2520–2536. <https://doi.org/10.1016/j.dsr2.2009.03.003>
- Horikawa, K., Martin, E., Basak, C., Onodera, J., Seki, O., Sakamoto, T., et al. (2015). Pliocene cooling enhanced by flow of low-salinity Bering Sea water to the Arctic Ocean. *Nature Communications*, 6(1), 7587. <https://doi.org/10.1038/ncomms8587>
- Huber, B., & Bahlburg, H. (2021). The provenance signal of climate–tectonic interactions in the evolving St. Elias orogen: Framework component analysis and pyroxene and epidote single grain geochemistry of sediments from IODP 341 sites U1417 and U1418. *International Journal of Earth Sciences*, 110(4), 1477–1499. <https://doi.org/10.1007/s00531-021-02025-9>
- Jaeger, J. M., Gulick, S. P. S., LeVay, L. J., Asahi, H., Bahlburg, H., Belanger, C. L., et al. (2014). Proceedings of the Integrated Ocean drilling Program. In *Expedition reports Southern Alaska margin*. Integrated Ocean Drilling Program. 341.
- Joh, Y., Di Lorenzo, E., Siqueira, L., & Kirtman, B. P. (2021). Enhanced interactions of Kuroshio Extension with tropical Pacific in a changing climate. *Scientific Reports*, 11(1), 6247. <https://doi.org/10.1038/s41598-021-85582-y>
- Kanazawa, A., Yoshioka, M., & Teshima, S.-I. (1971). The occurrence of brassicasterol in the diatoms *Cyclotella nana* and *Nitzschia Closterium*. *Bulletin of the Japanese Society of Scientific Fisheries*, 37(9), 889–903. <https://doi.org/10.2331/suisan.37.899>
- Katsuki, K., Takahashi, K., & Okada, M. (2003). Diatom assemblage and productivity changes during the last 340,000 Years in the subarctic Pacific. *Journal of Oceanography*, 59(5), 695–707. <https://doi.org/10.1023/b:joce.000009598.93075.78>
- Kipphut, G. K. (1990). Glacial meltwater input to the Alaska Coastal Current: Evidence from oxygen isotope measurements. *Journal of Geophysical Research*, 95(C4), 5177. <https://doi.org/10.1029/jc095ic04p05177>
- Knudson, K. P., Ravelo, A. C., Aiello, I. W., Knudson, C. P., Drake, M. K., & Sakamoto, T. (2021). Causes and timing of recurring subarctic Pacific hypoxia. *Science Advances*, 7(23), eabg2906. <https://doi.org/10.1126/sciadv.abg2906>
- Komar, N., & Zeebe, R. E. (2021). Reconciling atmospheric CO₂, weathering, and calcite compensation depth across the Cenozoic. *Science Advances*, 7(4), eabd4876. <https://doi.org/10.1126/sciadv.abd4876>
- Kornilova, O., & Rosell-Melé, A. (2003). Application of microwave-assisted extraction to the analysis of biomarker climate proxies in marine sediments. *Organic Geochemistry*, 34(11), 1517–1523. [https://doi.org/10.1016/s0146-6380\(03\)00155-4](https://doi.org/10.1016/s0146-6380(03)00155-4)
- Lam, A. R., & Leckie, R. M. (2020). Subtropical to temperate late neogene to quaternary planktic foraminiferal biostratigraphy across the Kuroshio current extension, shatsky rise, northwest Pacific ocean. *PLoS One*, 15(7), e0234351. <https://doi.org/10.1371/journal.pone.0234351>
- Lam, P. J., & Bishop, J. K. B. (2008). The continental margin is a key source of iron to the HNLC North Pacific Ocean. *Geophysical Research Letters*, 35(7). <https://doi.org/10.1029/2008GL033294>
- Lawrence, K. T., Herbert, T. D., Brown, C. M., Raymo, M. E., & Haywood, A. M. (2009). High-amplitude variations in North Atlantic sea surface temperature during the early Pliocene warm period. *Paleoceanography*, 24(2), PA2218. <https://doi.org/10.1029/2008PA001669>
- Lawrence, K. T., Liu, Z., & Herbert, T. D. (2006). Evolution of the eastern tropical Pacific through Plio-Pleistocene glaciation. *Science*, 312(5770), 79–83. <https://doi.org/10.1126/science.1120395>
- Lawrence, K. T., Sigman, D. M., Herbert, T. D., Riihimaki, C. A., Bolton, C. T., Martínez-García, A., et al. (2013). Time-transgressive North Atlantic productivity changes upon northern Hemisphere glaciation. *Paleoceanography*, 28(4), 740–751. <https://doi.org/10.1002/2013PA002546>
- Lei, Y., Servais, T., Feng, Q., & He, W. (2012). The spatial (nearshore–offshore) distribution of latest Permian phytoplankton from the Yangtze Block, South China. *Palaeogeography, Palaeoclimatology, Palaeoecology*, 363–364, 151–162. <https://doi.org/10.1016/j.palaeo.2012.09.010>
- Liu, J., Tian, J., Liu, Z., Herbert, T. D., Fedorov, A. V., & Lyle, M. (2019). Eastern equatorial Pacific cold tongue evolution since the late Miocene linked to extratropical climate. *Science Advances*, 5(4), eaau6060. <https://doi.org/10.1126/sciadv.aau6060>
- Liu, Z., Altabet, M. A., & Herbert, T. D. (2008). Plio-pleistocene denitrification in the eastern tropical north Pacific: Intensification at 2.1 Ma. *Geochemistry, Geophysics, Geosystems*, 9(11), Q11006. <https://doi.org/10.1029/2008GC002044>
- Liu, Z., & Herbert, T. D. (2004). High-latitude influence on the eastern equatorial Pacific climate in the early Pleistocene epoch. *Nature*, 427(6976), 720–723. <https://doi.org/10.1038/nature02338>
- Locarnini, R. A., Mishonov, A. V., Antonov, J. I., Boyer, T. P., Garcia, H. E., Baranova, O. K., et al. (2013). NOAA atlas NESDIS (Vol. 73). <https://doi.org/10.7289/V55X26VD>
- Lopes, C., Kucera, M., & Mix, A. C. (2015). Climate change decouples oceanic primary and export productivity and organic carbon burial. *Proceedings of the National Academy of Sciences*, 112(2), 332–335. <https://doi.org/10.1073/pnas.1410480111>
- Margalef, R. (1978). Life-forms of phytoplankton as survival alternatives in an unstable environment. *Oceanologica Acta*, 1, 493–508.
- Marlowe, I. T., Green, J. C., Neal, A. C., Brassell, S. C., Eglinton, G., & Course, P. A. (1984). Long-chain (n-C₃₇–C₃₉) alkenones in the Prymnesiophyceae. Distribution of alkenones and other lipids and their taxonomic significance. *British Phycological Journal*, 19(3), 203–216. <https://doi.org/10.1080/00071618400650221>

- Martin, J. H., & Fitzwater, S. E. (1988). Iron deficiency limits phytoplankton growth in the north-east Pacific subarctic. *Nature*, *331*(6154), 341–343. <https://doi.org/10.1038/331341a0>
- Martin, J. H., Gordon, R. M., Fitzwater, S., & Broenkow, W. W. (1989). VERTEX: Phytoplankton/iron studies in the Gulf of Alaska. *Deep-Sea Research*, *36*(5), 649–680. [https://doi.org/10.1016/0198-0149\(89\)90144-1](https://doi.org/10.1016/0198-0149(89)90144-1)
- Martin, J. H., Michael Gordon, R., & Fitzwater, S. E. (1991). Iron limitation? *Limnology & Oceanography*, *36*(8), 1793–1802. <https://doi.org/10.4319/lo.1991.36.8.1793>
- Martínez-Botí, M. A., Foster, G. L., Chalk, T. B., Rohling, E. J., Sexton, P. F., Lunt, D. J., et al. (2015). Plio-Pleistocene climate sensitivity valuated using high-resolution CO₂ records. *Nature*, *518*(7537), 49–54. <https://doi.org/10.1038/nature14145>
- Martínez-García, A., Rosell-Melé, A., McClymont, E. L., Gersonde, R., & Haug, G. (2010). Subpolar link to the emergence of the modern equatorial Pacific cold tongue. *Science*, *328*(5985), 1550–1553. <https://doi.org/10.1126/science.1184480>
- März, C., Schnetger, B., & Brumsack, H.-J. (2013). Nutrient leakage from the north Pacific to the Bering Sea (IODP site U1341) following the onset of northern hemispheric glaciation? *Paleoceanography*, *28*(1), 68–78. <https://doi.org/10.1002/palo.20011>
- Matthiesen, J., Knies, J., Vogt, C., & Stein, R. (2009). Pliocene palaeoceanography of the Arctic Ocean and subarctic seas. *Phil. Trans. R. Soc. A*, *367*(1886), 21–48. <https://doi.org/10.1098/rsta.2008.0203>
- McGee, D., Laws, R. A., & Cahoon, L. B. (2008). Live benthic diatoms from the upper continental slope: Extending the limits of marine primary production. *Marine Ecology Progress Series*, *356*, 103–112. <https://doi.org/10.3354/meps07280>
- Müller, J., Romero, O., Cowan, E. A., McClymont, E. L., Forwick, M., Asahi, H., et al. (2018). Cordilleran ice-sheet growth fuelled primary productivity in the Gulf of Alaska, northeast Pacific Ocean. *Geology*, *46*(4), 307–310. <https://doi.org/10.1130/g39904.1>
- Müller, P. J., & Schneider, R. R. (1993). An automated leaching method for the determination of opal in sediments and particulate matter. *Deep-Sea Research I*, *40*(3), 425–444. [https://doi.org/10.1016/0967-0637\(93\)90140-x](https://doi.org/10.1016/0967-0637(93)90140-x)
- Nakov, T., Beaulieu, J. M., & Alverson, A. J. (2019). Diatoms diversify and turn over faster in freshwater than marine environments. *Evolution*, *73*(12), 2497–2511. <https://doi.org/10.1111/evo.13832>
- Palevsky, H. I., Ribalet, F., Swallow, J. E., Cosca, C. E., Cokelet, E. D., Feely, R. A., et al. (2013). The influence of net community production and phytoplankton community structure on CO₂ uptake in the Gulf of Alaska. *Global Biogeochemical Cycles*, *27*(3), 664–676. <https://doi.org/10.1002/gbc.20058>
- Perry, S. E., Garver, J. I., & Ridway, K. D. (2009). Transport of the yakutat Terrane, southern Alaska: Evidence from sediment petrology and detrital zircon fission-track and U/Pb double dating. *The Journal of Geology*, *117*(2), 156–173. <https://doi.org/10.1086/596302>
- Piepho, M., Martin-Creuzburg, D., & Wacker, A. (2012). Phytoplankton sterol contents vary with temperature, phosphorus and silicate supply: A study on three freshwater species. *European Journal of Phycology*, *47*(2), 138–145. <https://doi.org/10.1080/09670262.2012.665484>
- Pisias, N. G., Mix, A. C., & Heusser, L. (2001). Millennial scale climate variability of the Northeast Pacific Ocean and Northwest North America based on Radiolaria and pollen. *Quaternary Science Reviews*, *20*(14), 1561–1576. [https://doi.org/10.1016/s0277-3791\(01\)00018-x](https://doi.org/10.1016/s0277-3791(01)00018-x)
- Pope, E. L., Talling, P. J., & Ó Cofaigh, C. (2018). The relationship between ice sheets and submarine mass movements in the Nordic Seas during the Quaternary. *Earth-Science Reviews*, *178*, 208–256. <https://doi.org/10.1016/j.earscirev.2018.01.007>
- Raja, M., & Rosell-Melé, A. (2021). Appraisal of sedimentary alkenones for the quantitative reconstruction of phytoplankton biomass. *Proceedings of the National Academy of Sciences*, *118*(2), 1–7. <https://doi.org/10.1073/pnas.2014787118>
- Rampen, S. W., Abbas, B. A., Schouten, S., & Sinninghe Damste, J. S. (2009). A comprehensive study of sterols in marine diatoms (Bacillariophyta): Implications for their use as tracers for diatom productivity. *Limnology & Oceanography*, *55*(1), 91–105. <https://doi.org/10.4319/lo.2010.55.1.0091>
- Rea, D. A., & Snoeckx, H. (1995). Sediment fluxes in the Gulf of Alaska; paleoceanographic record from site 887 on the Patton-Murray seamount platform. In D. K. Rea, L. A. Basov, D. W. Scholl, & J. F. Allan (Eds.) (Vol. 145, pp. 247–256). *Proc. ODP, Sci. Results*, Ocean Drilling Program.
- Rea, D. K., Basov, I. A., Krissiek, L. A., & the Leg 145 Scientific Party (1995). Scientific results of drilling the north Pacific transect. In D. K. Rea, I. A. Basov, D. W. Scholl, & J. F. Allan (Eds.), *Proceedings of the ocean drilling program* (Vol. 145). Scientific Results.
- Rea, D. K., Basov, L. A., Scholl, D. W., & Allan, J. F. (1995). Ocean Drilling Program. *Science Results*, *145*, 179–194. <https://doi.org/10.2973/odp.proc.sr.145.118.1995>
- Rea, D. K., & Snoeckx, H. (1993). Sediment fluxes in the Gulf of Alaska: Paleoceanographic record from site 887 on the Patton-Murray seamount platform. *Proceedings of the Ocean Drilling Program - Scientific Results*, *145*. <https://doi.org/10.2973/odp.proc.sr.145.122.1995>
- Ren, J., Gersonde, R., Esper, O., & Sancetta, C. (2014). Diatom distributions in northern North Pacific surface sediments and their relationship to modern environmental variables. *Palaeogeography, Palaeoclimatology, Palaeoecology*, *402*, 81–103. <https://doi.org/10.1016/j.palaeo.2014.03.008>
- Rieley, G., Collier, R. J., Jones, D. M., & Eglinton, G. (1991). The biogeochemistry of Ellesmere Lake, U.K.-I: Source correlation of leaf wax inputs to the sedimentary record. *Organic Geochemistry*, *17*, 901–912.
- Romero, O. E., Armand, L. K., Crosta, X., & Pichon, J. J. (2005). The biogeography of major diatom taxa in Southern Ocean surface sediments: 3. Tropical/subtropical species. *Palaeogeography, Palaeoclimatology, Palaeoecology*, *223*(1–2), 49–65. <https://doi.org/10.1016/j.palaeo.2005.03.027>
- Romero, O. E., Kim, J.-H., Bárcena, M. A., Hall, I. R., Zahn, R., & Schneider, R. (2015). High-latitude forcing of diatom productivity in the southern Agulhas Plateau during the past 350 kyr. *Paleoceanography*, *30*(2), 118–132. <https://doi.org/10.1002/2014pa002636>
- Romero, O. E., LeVay, L. J., McClymont, E. L., Müller, J., & Cowan, E. A. (2022). Orbital and suborbital-scale variations of productivity and sea surface conditions in the Gulf of Alaska during the past 54,000 Years: Impact of iron fertilization by icebergs and meltwater. *Paleoceanography and Paleoclimatology*, *37*(1), e2021PA004385. <https://doi.org/10.1029/2021PA004385>
- Romero, O. E., Mohtadi, M., Helmke, P., & Hebbeln, D. (2012). High interglacial diatom paleoproductivity in the westernmost Indo-Pacific warm pool during the past 130,000 yr. *Paleoceanography*, *27*(3), PA3209. <https://doi.org/10.1029/2012pa002299>
- Romero, O. E., Rixen, T., & Herunadi, B. (2009). Effects of hydrographic and climatic forcing on diatom production and export in the tropical southeastern Indian Ocean. *Marine Ecology Progress Series*, *384*, 69–82. <https://doi.org/10.3354/meps08013>
- Sancetta, C., & Calvert, S. E. (1988). The annual cycle of sedimentation in Saanich Inlet, British Columbia: Implications for the interpretation of diatom fossil assemblages. *Deep-Sea Research, Part A: Oceanographic Research Papers*, *35*(1), 71–90. [https://doi.org/10.1016/0198-0149\(88\)90058-1](https://doi.org/10.1016/0198-0149(88)90058-1)
- Sancetta, C., & Silvestri, S. M. (1986). Pliocene-Pleistocene evolution of the North Pacific ocean-atmospheric system, interpreted from fossil diatoms. *Paleoceanography*, *1*(2), 163–180. <https://doi.org/10.1029/pa001i002p00163>
- Sánchez-Montes, M. L., McClymont, E. L., Lloyd, J. M., Müller, J., Cowan, E. A., & Zorzi, C. (2019). Alkenone sea surface temperatures, ice rafted debris, terrestrial/aquatic n-alkane ratio, pollen counts and a new age and depth models from IODP Expedition 341 Site U1417, Gulf of Alaska. *PANGAEA*. <https://doi.org/10.1594/PANGAEA.899064>

- Sánchez-Montes, M. L., McClymont, E. L., Lloyd, J. M., Müller, J., Cowan, E. A., & Zorzi, C. (2020). Late Pliocene Cordilleran Ice Sheet development with warm northeast Pacific sea surface temperatures. *Climate of the Past*, *16*(1), 299–313. <https://doi.org/10.5194/cp-16-299-2020>
- Sánchez-Montes, M. L., Romero, O. E., Cowan, E. A., Müller, J., Moy, C. M., Lloyd, J. M., et al. (2021). Lipid biomarkers, siliceous microfossil assemblages, biogenic silica and carbon and nitrogen bulk and isotope analyses from IODP Hole 341-U1417D Gulf of Alaska [Dataset]. PANGAEA: <https://doi.org/10.1594/PANGAEA.936779>
- Schlitzer, R. (2016). Ocean Data view. Retrieved from <http://odv.awi.de>
- Schrader, H., & Gersonde, R. (1978). Diatoms and silicoflagellates. In *Zachariasse et al. Microplaeontological counting methods and techniques - an exercise on an eight metres section of the lower Pliocene of Capo Rossello, Sicily* (Vol. 17, pp. 129–176). Utrecht Micropal. Bull.
- Schroth, A. W., Crusius, J., Gassó, S., Moy, C. M., Buck, N. J., Resing, J. A., & Campbell, R. W. (2017). Atmospheric deposition of glacial iron in the Gulf of Alaska impacted by the position of the Aleutian Low. *Geophysical Research Letters*, *44*(10), 5053–5061. <https://doi.org/10.1002/2017gl073565>
- Seki, O., Foster, G. J., Schmidt, D. N., Mackensen, A., Kawamura, K., & Pancost, R. D. (2010). Alkenone and boron-based Pliocene pCO₂ records. *Earth and Planetary Science Letters*, *292*(1–2), 201–211. <https://doi.org/10.1016/j.epsl.2010.01.037>
- Shannon, C. E., & Weaver, W. (1949). *The mathematical theory of communication*. University of Illinois Press.
- Shimada, C., Sato, T., Yamasaki, M., Hasegawa, S., & Tanaka, Y. (2009). Drastic change in the late Pliocene subarctic Pacific diatom community associated with the onset of the Northern Hemisphere Glaciation. *Palaeogeography, Palaeoclimatology, Palaeoecology*, *279*(3–4), 207–215. <https://doi.org/10.1016/j.palaeo.2009.05.015>
- Sigman, D. M., Jaccard, S. L., & Haug, G. H. (2004). Polar ocean stratification in a cold climate. *Nature*, *428*(6978), 59–63. <https://doi.org/10.1038/nature02357>
- Studer, A. S., Martínez-García, A., Jaccard, S. L., Girault, F. E., Sigman, D. M., & Haug, G. H. (2012). Enhanced stratification and seasonality in the Subarctic Pacific upon Northern Hemisphere Glaciation—New evidence from diatom-bound nitrogen isotopes, alkenones and archaeal tetraethers. *Earth and Planetary Science Letters*, *351*–352, 84–94. <https://doi.org/10.1016/j.epsl.2012.07.029>
- Talling, P. J., Wynn, R. B., Masson, D. G., Frenz, M., Cronin, B. T., Schiebel, R., et al. (2007). Onset of submarine debris flow deposition far from original giant landslide. *Nature*, *450*, 541–544. <https://doi.org/10.1038/nature06313>
- Thunell, R. C., Pride, C. J., Tappa, E., & Muller-Karger, F. E. (1994). Biogenic silica fluxes and accumulation rates in the Gulf of California. *Geology*, *22*(4), 303–306. [https://doi.org/10.1130/0091-7613\(1994\)022<0303:BSFAAR>2.3.CO;2](https://doi.org/10.1130/0091-7613(1994)022<0303:BSFAAR>2.3.CO;2)
- Tsuda, A., Takeda, S., Saito, H., Nishioka, J., Nojiri, Y., Kudo, I., et al. (2003). A mesoscale iron enrichment in the Western subarctic Pacific induces a large centric diatom bloom. *Science*, *300*(5621), 958–961. <https://doi.org/10.1126/science.1082000>
- USGS (U.S. Geological Survey). (1981). Geographic names phase I data compilation (1976–1981). Geographic Names Information System Retrieved from <https://edit.nationalmap.gov/apps/gaz-domestic/public/summary/1413097>. last accessed 06 03 2022.
- Verardo, D. J., Froelich, P. N., & McIntyre, A. (1990). Determination of organic carbon and nitrogen in marine sediments using the Carlo Erba NA-1500. *Deep-Sea Research, Part I (Oceanographic Research Papers)*, *37*(1), 157–165. [https://doi.org/10.1016/0198-0149\(90\)90034-s](https://doi.org/10.1016/0198-0149(90)90034-s)
- Volkman, J. K. (1986). A review of sterol markers for marine and terrigenous organic matter. *Organic Geochemistry*, *9*(2), 83–99. [https://doi.org/10.1016/0146-6380\(86\)90089-6](https://doi.org/10.1016/0146-6380(86)90089-6)
- Volkman, J. K. (2006). Lipid markers for marine organic matter. In J. K. Volkman (Ed.), *Handbook of environmental chemistry* (Vol. 2, pp. 27–70). Springer-Verlag.
- Wakeham, S. G., Peterson, M. L., Hedges, J. I., & Lee, C. (2002). Lipid biomarker fluxes in the Arabian Sea, with a comparison to the equatorial Pacific Ocean. *Deep-Sea Research, Part 2, Topical Studies in Oceanography*, *49*(12), 2265–2301. [https://doi.org/10.1016/S0967-0645\(02\)00037-1](https://doi.org/10.1016/S0967-0645(02)00037-1)
- Walinsky, S. E., Prah, F. G., Mix, A. C., Finney, B. P., Jaeger, J. M., & Rosen, G. P. (2009). Distribution and composition of organic matter in surface sediments of coastal southeast Alaska. *Continental Shelf Research*, *29*(13), 1565–1579. <https://doi.org/10.1016/j.csr.2009.04.006>
- Walton, M. A. L., Gulick, S. P. S., Reece, R. S., Barth, G. A., Christeson, G. L., & Van Avendonk, H. J. A. (2014). Dynamic response to strike-slip tectonic control on the deposition and evolution of the Baranof Fan, Gulf of Alaska. *Geosphere*, *10*(4), 680–691. <https://doi.org/10.1130/GES01034.1>
- Wang, K. J., Huang, Y., Majaneva, M., Belt, S. T., Liao, S., Novak, J., et al. (2021). Group 2i Isochrysidales produce characteristic alkenones reflecting sea ice distribution. *Nature Communications*, *12*(1), 15. <https://doi.org/10.1038/s41467-020-20187-z>
- Weingartner, T. (2007). Chapter 2.2: The physical environment of the Gulf of Alaska. In R. B. Spies (Ed.), *Long-term ecological change in the northern Gulf of Alaska*. Elsevier, 589.
- Whitney, F. A., Crawford, D. W., & Yoshimura, T. (2005). The uptake and export of silicon and nitrogen in HNLC waters of the NE Pacific Ocean. *Deep-Sea Research, Part II*, *52*(7–8), 1055–1067. <https://doi.org/10.1016/j.dsr2.2005.02.006>
- Williamson, P., & Holligan, P. M. (1990). Ocean productivity and climate change. *Trends in Ecology & Evolution*, *5*(9), 299–303. [https://doi.org/10.1016/0169-5347\(90\)90085-r](https://doi.org/10.1016/0169-5347(90)90085-r)
- Zdanowicz, C., Hall, G., Vaive, J., Amelin, Y., Percival, J., Girard, I., et al. (2006). Asian dust fall in the St. Elias mountains, Yukon, Canada. *Geochimica et Cosmochimica Acta*, *70*(14), 3493–3507. <https://doi.org/10.1016/j.gca.2006.05.005>
- Zindorf, M., März, C., Wagner, T., Gulick, S. P. S., Strauss, H., Benowitz, J., et al. (2019). Deep sulfate-Methane-transition and sediment diagenesis in the Gulf of Alaska (IODP site U1417). *Marine Geology*, *417*, 105986. <https://doi.org/10.1016/j.margeo.2019.105986>
- Zindorf, M., Rush, D., Jaeger, J., Mix, A., Penkrot, M. L., Schnetger, B., et al. (2020). Reconstructing oxygen deficiency in the glacial Gulf of Alaska: Combining biomarkers and trace metals as paleo-redox proxies. *Chemical Geology*, *558*, 119864. <https://doi.org/10.1016/j.chemgeo.2020.119864>